

Improving Sampling Accuracy of Stochastic Gradient MCMC Methods via Non-uniform Subsampling of Gradients

Ruilin Li¹, Xin Wang², Hongyuan Zha¹, Molei Tao¹

Georgia Institute of Technology¹
Google Inc.²

June 17, 2022

Abstract

Common Stochastic Gradient MCMC methods approximate gradients by stochastic ones via uniformly subsampled data points. We propose that a non-uniform subsampling can reduce the variance introduced by the stochastic approximation, hence making the sampling of a target distribution more accurate. An exponentially weighted stochastic gradient approach (EWSG) is developed for this objective by matching the transition kernels of SG-MCMC methods respectively based on stochastic and batch gradients. A demonstration of EWSG combined with second-order Langevin equation for sampling purposes is provided. In our method, non-uniform subsampling is done efficiently via a Metropolis-Hastings chain on the data index, which is coupled to the sampling algorithm. The fact that our method has reduced local variance with high probability is theoretically analyzed. A non-asymptotic global error analysis is also presented. Numerical experiments based on both synthetic and real world data sets are also provided to demonstrate the efficacy of the proposed approaches. While statistical accuracy has improved, the speed of convergence was empirically observed to be at least comparable to the uniform version.

1 Introduction

Many MCMC methods use physics-inspired evolution such as Langevin dynamics [8] to utilize gradient information for exploring posterior distributions over continuous parameter space more efficiently. However, gradient-based MCMC methods are often limited by the computational cost of computing the gradient on large data sets. Motivated by the great success of stochastic gradient methods for optimization problems, stochastic gradient MCMC methods (SG-MCMC) for sampling distributions have also been gaining increasing attention. When the accurate but expensive-to-evaluate batch gradients in a MCMC method are replaced by computationally cheaper estimates based on a subset of the data, the method is turned to a stochastic gradient version. Successful examples include SG (overdamped) Langevin Dynamics [33] and SG Hamiltonian Monte Carlo [10], all of which were designed for scalability suitable for machine learning tasks.

However, directly replacing the batch gradient by a (uniform) stochastic one without additional mitigation will generally cause a MCMC method to sample from a statistical distribution different from the target, because the transition kernel of the MCMC method gets corrupted by the noise of subsampled gradient. In general, the additional noise is tolerable if the learning rate/step size is tiny or decreasing. However, when large step are used, the extra noise is non-negligible and undermines the performance of downstream applications such as Bayesian inference.

In this paper, we present a state-dependent non-uniform SG-MCMC algorithm termed exponentially weighted stochastic gradients method (EWSG), which is in line with the efforts of uniform SG-MCMC methods for better scalability. The novelty of our approach is, unlike uniform gradient subsampling approaches which aim only at an unbiased gradient estimator, our approach is motivated by directly matching the transition kernel of a SG-MCMC method with the transition kernel of a full-gradient-based MCMC method, and this matching naturally leads to EWSG algorithm. All SG-MCMC methods

contain two sources of stochasticity, one being the intrinsic randomness of MCMC, and the other being the randomness introduced by gradient subsampling. In conventional treatments where uniform gradient subsampling is used, the latter randomness is independent of the former one, and thus when they are coupled together, variances add up. EWSG, on the other hand, dynamically chooses the weight of each datum according to the current state of the MCMC, and is able to keep the transition kernel of the Markov process to be close to that of a gradient-based MCMC method with full gradient. Therefore, the invariant distribution of EWSG (if existent) will be close to that of a full-gradient based MCMC method, and this is how better accuracy in sampling the target distribution can be achieved.

Our presentation of EWSG will be based on second-order Langevin equations, although it works for other MCMC methods too (e.g., Sec.F). To concentrate on the role of non-uniform weights when approximating the full-gradient by a stochastic version, we will work with constant step sizes/learning rate only. The fact that EWSG has locally reduced variance than its uniform counterpart is rigorously argued in Theorem 3 and a global non-asymptotic analysis of EWSG is given in Theorem 4 to show its convergence properties and demonstrate the advantage over its uniform stochastic gradient counterpart.

A number of experiments on synthetic and real world data sets, across various downstream machine learning tasks, including Bayesian logistic regression and Bayesian neural networks, are conducted to validate our theoretical results and demonstrate the effectiveness of EWSG. In addition to improved statistical accuracy, the speed of convergence was empirically observed, in a fair comparison setup based on the same data pass, to be at least comparable to, and in some cases faster than, its uniform counterpart. Additional theoretical investigation of convergence speed of EWSG is provided in Section H in appendix.

2 Related Work

2.1 Stochastic Gradient MCMC Methods

Since the seminal work of SGLD [33], which joined the forces of stochastic gradient and gradient-based MCMC methods, much progress has been made. [1] proposed modification of SGLD which samples from a Gaussian approximation of posterior. [26] extended SGLD to Riemann manifolds. [31] theoretically justified convergence of SGLD and gave practical recommendation for tuning step size. [19] introduced preconditioner and greatly improved stability of SGLD. We also refer to [22] and [15] which will be discussed in Sec.5. While these work were mostly based on first-order (overdamped) Langevin dynamics, other dynamics were considered too; for instance, [10] proposed SGHMC, which is closely related to second-order (underdamped) Langevin dynamics [7, 5]. Second-order Langevin dynamics is faster than the first-order version in certain situations [12, 11] and starts to gain more attention in the machine learning community.

2.2 Variance Reduction

Vanilla stochastic gradient methods usually find approximate solutions relatively quickly but the convergence speed slows down when an accurate solution is needed [2, 17]. Stochastic average gradient algorithm [30] improved the convergence speed of stochastic gradient methods to linear, which is the same as gradient descent methods with full gradient, at the expense of large memory overhead. Stochastic variance reduced gradient (SVRG) [17] successfully reduced this memory overhead. [14] applied variance reduction technique to SGLD and obtained a tighter bound.

EWSG is effective in reducing the variance introduced by the stochastic gradient; however, it is based on a new idea — matching transition kernels of MCMC. It thus can be combined with traditional VR approaches (e.g., Sec.G).

2.3 Importance Sampling

Importance sampling, when combined with stochastic gradient methods, is a useful technique to reduce variance. Stochastic gradient methods with static importance sampling fix a probability distribution which do not change along iterations. However, computing the fixed distribution often requires prior

information of gradient terms, e.g. Lipschitz constants, upper bounds, or γ -smoothness [25, 29, 13], which could be difficult to compute or estimate. On the other hand, stochastic gradient methods with adaptive importance sampling re-evaluate the importance at each iteration, whose computation usually requires the entire data set per parameter update [35, 36].

The proposed approach can be categorized as an adaptive importance sampling method. However, it does not require the full data set per parameter update; instead, an inner-loop Metropolis chain was designed for a random data index to approximate a state-dependent non-uniform distribution.

3 Background

Underdamped Langevin Dynamics is described by a diffusion process governed by the following SDE

$$\begin{cases} d\boldsymbol{\theta} = \mathbf{r} dt \\ d\mathbf{r} = -(\nabla V(\boldsymbol{\theta}) + \gamma \mathbf{r}) dt + \sigma d\mathbf{W} \end{cases} \quad (1)$$

where $\boldsymbol{\theta} \in \mathbb{R}^d$ is a state (position) variable, $\mathbf{r} \in \mathbb{R}^d$ is a momentum variable, V is a potential energy function which in our context (originated from cost minimization or Bayesian inference over many data) is the sum of many terms $V(\boldsymbol{\theta}) = \sum_{i=1}^n V_i(\boldsymbol{\theta})$, γ is friction coefficient, σ is intrinsic noise amplitude, and \mathbf{W} is a standard multi-dimensional Wiener process. Under mild assumptions on the potential V (e.g., [27]), Langevin dynamics admits a unique invariant distribution

$$\pi(\boldsymbol{\theta}, \mathbf{r}) = Z^{-1} \exp\left(-\frac{1}{T}(V(\boldsymbol{\theta}) + \frac{\|\mathbf{r}\|^2}{2})\right) \quad (2)$$

and is in many cases geometric ergodic, where Z is a normalization constant and T is the temperature of system determined by friction and noise via the fluctuation dissipation theorem $\sigma^2 = 2\gamma T$ [18].

The main reason for considering underdamped Langevin rather than overdamped one is that underdamped Langevin can converge faster than overdamped Langevin, in particular in high-dimension space [12]. Like the overdamped version, numerical integrators for underdamped Langevin with well captured statistical properties of the continuous process have been extensively investigated [28, 6], and both the overdamped and underdamped integrators are friendly to derivations that will allow us to obtain explicit expressions of the non-uniform weights.

Terminology-wise, ∇V will be called the full/batch-gradient, $n\nabla V_I$ with random I will be called stochastic gradient (SG), and when I is uniform distributed it will be called a uniform SG/subsampling, otherwise non-uniform. When uniform SG is used to approximate the batch-gradient in underdamped Langevin, the method will be referred to as (vanilla) stochastic gradient underdamped Langevin dynamics (**SGULD**), and it serves as a baseline in experiments.

4 Main Work

4.1 Non-optimality of Uniform Subsampling

Uniform subsampling of gradients have long been the dominant way of stochastic gradient approximations. In many machine learning applications, cases where data size n is much larger than problem dimension d are not uncommon. In such cases, $\{\nabla V_i\}_{i=1,2,\dots,n} \subset \mathbb{R}^d$ are linearly dependent and hence it is possible that there exist probability distributions $\{p_i\}_{i=1,2,\dots,n}$ other than the uniform one such that the gradient estimate is unbiased. This opens up the door to develop non-uniform subsampling schemes (weights may be $\boldsymbol{\theta}$ dependent), which can help reduce introduced additional variance while maintaining unbiasedness.

In fact, in a reasonable setup, it turns out an optimal way of subsampling gradients, is far from being uniform:

Theorem 1 Suppose given $\boldsymbol{\theta} \in \mathbb{R}^d$, the errors of stochastic gradient approximation

$$\mathbf{b}_i = n\nabla V_i(\boldsymbol{\theta}) - \nabla V(\boldsymbol{\theta}), \quad i = 1, 2, \dots, n$$

are i.i.d. absolutely continuous random vectors with possibly- $\boldsymbol{\theta}$ -dependent density $p(x|\boldsymbol{\theta})$. Define $\mathbf{p} \in \mathbb{R}^n$ as a sparse vector if the number of non-zero entries in \mathbf{p} is no greater than $d+1$. Then with probability 1, the optimal probability distribution \mathbf{p}^* that is unbiased and minimizes the trace of the covariance of $n\nabla V_I(\boldsymbol{\theta})$, i.e. \mathbf{p}^* which solves

$$\min_{\mathbf{p}} \text{Tr}(\mathbb{E}_{I \sim \mathbf{p}}[\mathbf{b}_I \mathbf{b}_I^T]) \quad \text{s.t. } \mathbb{E}_{I \sim \mathbf{p}}[\mathbf{b}_I] = \mathbf{0}, \quad (3)$$

is a sparse vector.

Despite the sparsity of \mathbf{p}^* , which seemingly suggests that one only needs to use at most $d+1$ gradient terms (which $d+1$ terms may vary across iterations) when using stochastic gradient methods, it is not practical because \mathbf{p}^* requires solving the linear programming problem (3) in Theorem 1, for which an entire data pass is needed. Nevertheless, this result still shows uniform gradient subsampling can be far from optimal and motivates us to propose an exponentially weighted stochastic gradient method, which has reduced local variance with high probability and at the same time remains efficiently implementable without necessarily using all the data per parameter update.

4.2 Exponentially Weighted Stochastic Gradient

MCMC methods or Markov processes in general are characterized by their transition kernels. In traditional SG-MCMC methods, uniform gradient subsampling is used, which is completely independent of the intrinsic randomness of MCMC methods (e.g. diffusion in underdamped Langevin), as a result, the transition kernel of SG-MCMC method can be quite different from gradient-based MCMC methods with full gradient. Therefore, it is natural to ask - is it possible to couple these two originally independent randomness so that the transition kernels can be better matched and the sampling accuracy can be hence improved?

Consider Euler-Maruyama (EM) discretization¹ of eq. (1):

$$\begin{cases} \boldsymbol{\theta}_{k+1} = \boldsymbol{\theta}_k + \mathbf{r}_k h \\ \mathbf{r}_{k+1} = \mathbf{r}_k - (\nabla V(\boldsymbol{\theta}_k) + \gamma \mathbf{r}_k)h + \sigma \sqrt{h} \boldsymbol{\xi}_{k+1} \end{cases} \quad (4)$$

where h is step size and $\boldsymbol{\xi}_{k+1}$'s are i.i.d. d -dimensional standard Gaussian random variables.

Denote the transition kernel of EM discretization with full gradient by $P^{EM}(\boldsymbol{\theta}_{k+1}, \mathbf{r}_{k+1} | \boldsymbol{\theta}_k, \mathbf{r}_k)$. If $\nabla V(\boldsymbol{\theta}_k)$ is replaced by a weighted stochastic gradient $n\nabla V_{I_k}(\boldsymbol{\theta}_k)$, where I_k is the index of datum chosen to approximate full gradient and has probability mass function $\mathbb{P}(I_k = i) = p_i$, denote the transition kernel by $\tilde{P}^{EM}(\boldsymbol{\theta}_{k+1}, \mathbf{r}_{k+1} | \boldsymbol{\theta}_k, \mathbf{r}_k)$.

It turns out that we can choose p_i in a smart way to match the two transition kernels:

Theorem 2 Denote $\mathbf{x} = \frac{\mathbf{r}_{k+1} - \mathbf{r}_k + h\gamma \mathbf{r}_k}{\sigma \sqrt{h}}$ and $\mathbf{a}_i = \frac{\sqrt{h} \nabla V_i(\boldsymbol{\theta}_k)}{\sigma}$. If we set

$$p_i = \hat{Z}^{-1} \exp \left\{ -\frac{\|\mathbf{x} + \sum_{j=1}^n \mathbf{a}_j\|^2}{2} + \frac{\|\mathbf{x} + n\mathbf{a}_i\|^2}{2} \right\} \quad (5)$$

where \hat{Z} is a normalization constant, then the two transition kernels are identical, i.e.,

$$\tilde{P}^{EM}(\boldsymbol{\theta}_{k+1}, \mathbf{r}_{k+1} | \boldsymbol{\theta}_k, \mathbf{r}_k) = P^{EM}(\boldsymbol{\theta}_{k+1}, \mathbf{r}_{k+1} | \boldsymbol{\theta}_k, \mathbf{r}_k)$$

We refer to this choice of p_i Exponentially Weighted Stochastic Gradient (**EWSG**). Note the idea of designing non-uniform weights of stochastic gradient MCMC to match the transition kernel of full gradient can be suitably applied to a wide class of gradient-based MCMC methods; for example, Sec.F shows how EWSG can be applied to Langevin Monte Carlo (overdamped Langevin equation). In this sense, EWSG is complementary to a wide range of classical and contemporary SG-MCMC approaches.

Compared with vanilla stochastic gradients, exponentially weighted stochastic gradients have smaller variance with high probability, as is shown in Theorem 3.

¹Euler-Maruyama is not the most accurate or robust discretization, see e.g., [28, 6], but since it may still be the most used method, demonstrations in this article will be based on EM. Nevertheless, the same idea of EWSG can be easily applied to most other discretizations such as Geometric Langevin Algorithm [6].

Theorem 3 Assume $\{\nabla V_i(\boldsymbol{\theta})\}_{i=1,2,\dots,n}$ are i.i.d random vectors and $|\nabla V_i(\boldsymbol{\theta})| \leq R$ for some constant R almost surely. Denote the uniform distribution over $\{1, \dots, n\}$ by \mathbf{p}^U , the exponentially weighted distribution by \mathbf{p}^E , and let $\Delta = \text{Tr}[\text{cov}_{I \sim \mathbf{p}^E}[n \nabla V_I(\boldsymbol{\theta}) | \boldsymbol{\theta}] - \text{cov}_{I \sim \mathbf{p}^U}[n \nabla V_I(\boldsymbol{\theta}) | \boldsymbol{\theta}]]$. If $\mathbf{x} = \mathcal{O}(\sqrt{h})$, we have

$$\mathbb{E}[\Delta] < 0,$$

and $\exists C > 0$ independent of n or h such that for any $\epsilon > 0$

$$\mathbb{P}(|\Delta - \mathbb{E}[\Delta]| \geq \epsilon) \leq 2 \exp\left(-\frac{\epsilon^2}{nCh^2}\right)$$

Intuitively, less nonintrinsic local variance means better global statistical accuracy, and this reasoning will be made more rigorous in Section 4.4.

4.3 Practical Implementation

In EWSG, the probability of each gradient term is

$$p_i = \hat{Z}^{-1} \exp\left\{-\frac{\|\mathbf{x} + \sum_{j=1}^n \mathbf{a}_j\|^2}{2} + \frac{\|\mathbf{x} + n\mathbf{a}_i\|^2}{2}\right\}$$

Although the term $\|\mathbf{x} + \sum_{j=1}^n \mathbf{a}_j\|^2/2$ depends on the full data set, it is shared by all p_i 's and can be absorbed into the normalization constant \hat{Z}^{-1} (we still included it explicitly due to the needs of analyses in proofs); unique to each p_i is only the term $\|\mathbf{x} + n\mathbf{a}_i\|^2/2$, which involves only one data point. This motivates us to run a Metropolis-Hastings chain over the possible indices $i \in \{1, 2, \dots, n\}$: at each inner-loop step, a proposal of index value j will be uniformly drawn, and then accepted with probability

$$P(i \rightarrow j) = \min\left\{1, \exp\left(\frac{\|\mathbf{x} + n\mathbf{a}_j\|^2}{2} - \frac{\|\mathbf{x} + n\mathbf{a}_i\|^2}{2}\right)\right\}; \quad (6)$$

if accepted, the current index value i will be replaced by j . When this Markov chain converges, it is easy to see the index will follow the distribution given by p_i . The advantage is, we avoid explicitly passing through the entire data sets to compute each p_i , but yet the index will still sample from the non-uniform distribution efficiently.

In practice, we often only perform $M = 1$ step of the Metropolis chain per integration step, especially if h is not too large. The rationale is, when h is small, the integration timescale is slower than the index chain timescale. Note although the efficacy of local variance reduction via non-uniform subsampling is more pronounced when h is larger (see e.g., Theorem 4), in which case $M = 1$ may no longer be the optimal choice, improved sampling with large h and $M = 1$ is still clearly observed in numerical experiments with various sampling/learning tasks (Section 5).

Another hyper-parameter is \mathbf{x} , because p_i essentially depends on the future state $\boldsymbol{\theta}_{k+1}$ via \mathbf{x} , which we do not know, and yet we'd like to avoid expensive nonlinear solves. Therefore, in our experiments, we choose $\mathbf{x} = \frac{\sqrt{h}\mathbf{r}_k}{\sigma}$. That corresponds to a deterministic MLE of $\mathbf{r}_{k+1} = \mathbf{r}_k$, which is a sufficient (but not necessary) condition for mimicking the statistical equilibrium at which \mathbf{r}_{k+1} and \mathbf{r}_k are equal in distribution. This approximation turned out to be a good one in all our experiments with medium h and $M = 1$. Because it is only an approximation, when h is large, the method still introduces extra variance (smaller than that caused by vanilla stochastic gradient variant, though), and larger M may actually decrease the accuracy of sampling.

EWSG algorithm is summarized in Algorithm 1. For simplicity of notation, we restrict the description to the stochastic gradient case (i.e., mini batch size $b = 1$), but an extension to $b > 1$ (i.e. minibatch SG) is straightforward via multidimensional random indices I_1, \dots, I_b . See Section E in appendix for details.

EWSG has reduced variance but does not completely eliminate the nonintrinsic noise created by stochastic gradient due to these approximations. A small bias was also created by these approximations, but its effect is dominated by the variance effect (see Sec.4.4). In practice, if needed, one can combine EWSG with other variance reduction technique to further improve accuracy. We showcase how EWSG can be combined with SVRG in Sec.G of appendix.

Algorithm 1 EWSG

Input: {the number of data terms n , corresponding gradient functions $V_i(\cdot)$, $i = 1, 2, \dots, n$, step size h , the number of data passes K , index chain length M , friction and noise coefficients γ and σ }
 Initialize $\boldsymbol{\theta}_0, \mathbf{r}_0$ (arbitrarily, or use an informed guess)
for $k = 0, 1, \dots, \lceil \frac{Kn}{M+1} \rceil$ **do**
 $i \leftarrow$ uniformly sampled from $1, \dots, n$, compute and store $n\nabla V_i(\boldsymbol{\theta}_k)$
 $I \leftarrow i$
for $m = 1, 2, \dots, M$ **do**
 $j \leftarrow$ uniformly sampled from $1, \dots, n$, compute and store $n\nabla V_j(\boldsymbol{\theta}_k)$
 $I \leftarrow j$ with probability in Equation 6
end for
 Evaluate $\tilde{V}(\boldsymbol{\theta}_k) = nV_I(\boldsymbol{\theta}_k)$
 Update $(\boldsymbol{\theta}_{k+1}, \mathbf{r}_{k+1}) \leftarrow (\boldsymbol{\theta}_k, \mathbf{r}_k)$ via one step of Euler-Maruyama integration using $\tilde{V}(\boldsymbol{\theta}_k)$
end for

4.4 Theoretical Analysis

We now provide a non-asymptotic analysis of the global sampling error of EWSG. We first define some notations and list the required assumptions, and then state the main results. Detailed proof are deferred to appendix.

The generator \mathcal{L} of underdamped Langevin (1) is given by

$$\mathcal{L}f(\mathbf{X}_t) = (\mathbf{r}^T \nabla_{\boldsymbol{\theta}} - (\gamma \mathbf{r} + \nabla V(\boldsymbol{\theta}))^T \nabla_{\mathbf{r}} + \gamma \Delta_{\mathbf{r}})f(\mathbf{X}_t)$$

where $\mathbf{X} = (\boldsymbol{\theta}^T, \mathbf{r}^T)^T \in \mathbb{R}^{2d}$. \mathcal{L} is associated with an integrated form via Kolmogorov's backward equation $\mathbb{E}[f(\mathbf{X}_t)] = e^{t\mathcal{L}}f(\mathbf{X}_0)$. Given a test function $\phi(\mathbf{x})$, its posterior average is given by $\bar{\phi} = \int \phi(\mathbf{x})\pi(\mathbf{x})d\mathbf{x}$, where $\pi(\mathbf{x})$ is the invariant distribution defined in Eq. (2), and we use the time average of samples $\hat{\phi}_K = \frac{1}{K} \sum_{k=1}^K \phi(\mathbf{X}_k^E)$ to approximate $\bar{\phi}$, where \mathbf{X}_k^E is the sample path of a Markov chain (e.g., given by EM integrator). A useful tool in weak convergence analysis for SG-MCMC is the following Poisson equation [24, 32, 9]:

$$\mathcal{L}\psi = \phi - \bar{\phi} \tag{7}$$

The solution function ψ characterizes the difference between test function ϕ and its posterior average $\bar{\phi}$.

We make the following three assumptions:

Assumption 1 (Bounded Gradient of Potential) *The gradient of the all potential terms are uniformly bounded*

$$\|n\nabla V_i(\boldsymbol{\theta})\|_2 < M_1, \forall i = 1, 2, \dots, n, \boldsymbol{\theta} \in \mathbb{R}^d$$

Hence we also have $\|\nabla V(\boldsymbol{\theta})\| = \|\sum_{i=1}^n V_i(\boldsymbol{\theta})\| < M_1$.

Assumption 2 (Bounded Moments of Momentum) *Assume the p -th moment of the momentum variable \mathbf{r}_k^E are uniformly bounded across all iterations*

$$\mathbb{E}[\|\mathbf{r}_k^E\|^p] < M_2, \forall k = 0, 1, 2, \dots,$$

Hence by Holder's inequality, all lower moments are also uniformly bounded. In our proof, we require $p = 8$.

Assumption 3 (Bounded Solution of Poisson Equation) *The solution ψ of the Possion equation and all of its q -th order derivative are uniformly bounded*

$$\|D^l \psi\|_{\infty} < M_3, \forall l = 0, 1, \dots, q$$

We need $q = 3$ in our proof.

We are now ready to bound the mean squared error (MSE) for stochastic gradient underdamped Langevin algorithms, including both SGULD and the proposed EWSG algorithm.

Theorem 4 Under Assumption 1, 2 and 3, for both SGULD and EWSG algorithms, there exists a constant $C > 0$ such that

$$\mathbb{E}(\hat{\phi}_K - \bar{\phi})^2 \leq C\left(\frac{1}{T} + \frac{h}{T} \frac{\sum_{k=0}^{K-1} \mathbb{E}[\text{Tr}[\text{cov}(n \nabla V_{I_k} | \mathcal{F}_k)]]}{K} + h^2\right) \quad (8)$$

where $T = Kh$ is the corresponding time in the underlying continuous dynamics, I_k is the index of the datum used to estimate gradient at k -th iteration, and $\text{cov}(n \nabla V_{I_k} | \mathcal{F}_k)$ is the covariance of stochastic gradient at k -th iteration conditioned on the current sigma algebra \mathcal{F}_k in the filtration.

Remark: We follow the powerful framework developed in [24] to prove this bound, and to this end, our notations in the proof are made consistent to theirs. One key difference is, [24] only discusses the batch gradient case, whereas our theory has an additional quantification of the effect of non-uniform stochastic gradient. Note [32, 9] studied the effect of stochastic gradient, but the SG considered there did not use state-dependent weights, which would destroy several martingales used in their proofs. In addition, our result incorporates the effects of both local bias and local variance of a SG approximation. Unlike in [24] but like in [32, 9], our state space is not the compact set of torus but \mathbb{R}^d .

Variance and bias of the stochastic gradient approximation were respectively reflected in the 2nd and 3rd term in the above bound, although the 3rd term also contains a contribution from the numerical integration error. Note the 2nd term is larger than the 3rd in general due to its lower order in h , which means reducing the local variance can improve the sampling accuracy even if this is at the cost of introducing a small bias. Having a smaller local variance is the main advantage of EWSG over uniform SG (see e.g., Thm.3).

5 Experiments

In this section, the proposed EWSG algorithm will be compared with SGULD, the classical SGLD method [33], as well as several recent popular SG-MCMC methods, including Firefly Monte Carlo (FlyMC) [22], pSGLD [19], and CP-SG-MCMC [15] (this one is motivated by combining importance sampling with SG-MCMC). Test problems will include sampling from a simple Gaussian distribution, fitting a misspecified Gaussian model, Bayesian logistic regression, and Bayesian neural network(BNN). As FlyMC requires a tight lower bound of likelihood, which is unknown for many models, it will only be compared against in Sec. 5.2 and 5.3 where such a bound is obtainable. CP-SG-MCMC requires heavy tuning on the number of clusters which differs across data sets/algorithms, so it will only be included in the BNN example, for which the authors empirically found such a good hyper parameter for MNIST.

For fair comparison, all algorithms use constant step sizes and are allowed fixed computation budget, i.e., for L data passes, all algorithms are only allowed to call gradient function nL times. All experiments are conducted on a machine with a 2.20GHz Intel(R) Xeon(R) E5-2630 v4 CPU and an Nvidia GeForce GTX 1080 GPU. If not specifically mentioned, the noise coefficient is set $\sigma = \sqrt{2\gamma}$ so only γ needs to be specified in each experiment, the length of the index chain is set $M = 1$ for EWSG and the default value of two hyper-parameters required in pSGLD are set $\lambda = 10^{-5}$ and $\alpha = 0.99$, the same as suggested in [19].

5.1 A Simple Gaussian Example

Consider sampling from a simple two-dimensional Gaussian distribution whose potential function is $V(\boldsymbol{\theta}) = \sum_{i=1}^n V_i(\boldsymbol{\theta}) = \sum_{i=1}^n \frac{1}{2} \|\boldsymbol{\theta} - \mathbf{c}_i\|^2$. In this experiment, we set $n = 20$, and randomly sample $\mathbf{c}_i, i = 1, 2, \dots, n$ from a two-dimensional standard normal $\mathcal{N}(\mathbf{0}, I_2)$. Due to the simplicity of $V(\boldsymbol{\theta})$, we can write the target density analytically as $p(\boldsymbol{\theta}) \sim N(\frac{1}{n} \sum_{i=1}^n \mathbf{c}_i, \frac{1}{n} I_2)$, and are able to report sample quality quantitatively and compare it with vanilla stochastic gradient method on an objective basis. To this end, we use Kullback-Leibler divergence $\text{KL}(p\|q) = \int p(\boldsymbol{\theta}) \log \frac{p(\boldsymbol{\theta})}{q(\boldsymbol{\theta})} d\boldsymbol{\theta}$ to measure how different the target distribution and samples generated by simulation are. For two Gaussians, we have closed form expression for KL divergence $\text{KL}(p\|q) = \frac{1}{2} \left(\text{Tr}(\Sigma_2^{-1} \Sigma_1) + (\mu_2 - \mu_1)^\top \Sigma_2^{-1} (\mu_2 - \mu_1) - d + \ln \frac{|\Sigma_2|}{|\Sigma_1|} \right)$

where $p \sim N(\mu_1, \Sigma_1)$, $q \sim N(\mu_2, \Sigma_2)$. The formula is used to estimate the KL divergence between generated samples and the target distribution.

For each algorithm, we generate 10000 independent samples. All algorithms are run for 30 data passes and minibatch size of 1 is used for all of them. Step size is tuned from $5 \times \{10^{-1}, 10^{-2}, 10^{-3}\}$ and 5×10^{-3} is chosen for SGLD and pSGLD, 5×10^{-2} is chosen for SGULD and EWSG. For SGULD and EWSG, both of which are based on underdamped Langevin, we set friction coefficient $\gamma = 10$. The results are shown in Figure 1(a). From the figure, we observe that both SGULD and EWSG outperform the other two benchmarks SGLD and pSGLD. Between the two, EWSG converges to a smaller KL divergence than SGULD, which implies EWSG achieves better statistical accuracy than its uniform stochastic gradient counterpart.

We also consider comparing SGULD and EWSG at a large range of different step sizes, and plot the mean absolute error of sample covariance matrix against autocorrelation time² in Figure 1(b). When simulating a gradient-based Markov chain, generally speaking, large step size reduces autocorrelation time, yet leads to large discretization error. We observe from Figure 1(b) that at the same autocorrelation time, EWSG achieves smaller error of covariance estimate than SGULD, which demonstrates the effectiveness of EWSG from a more statistical perspective.

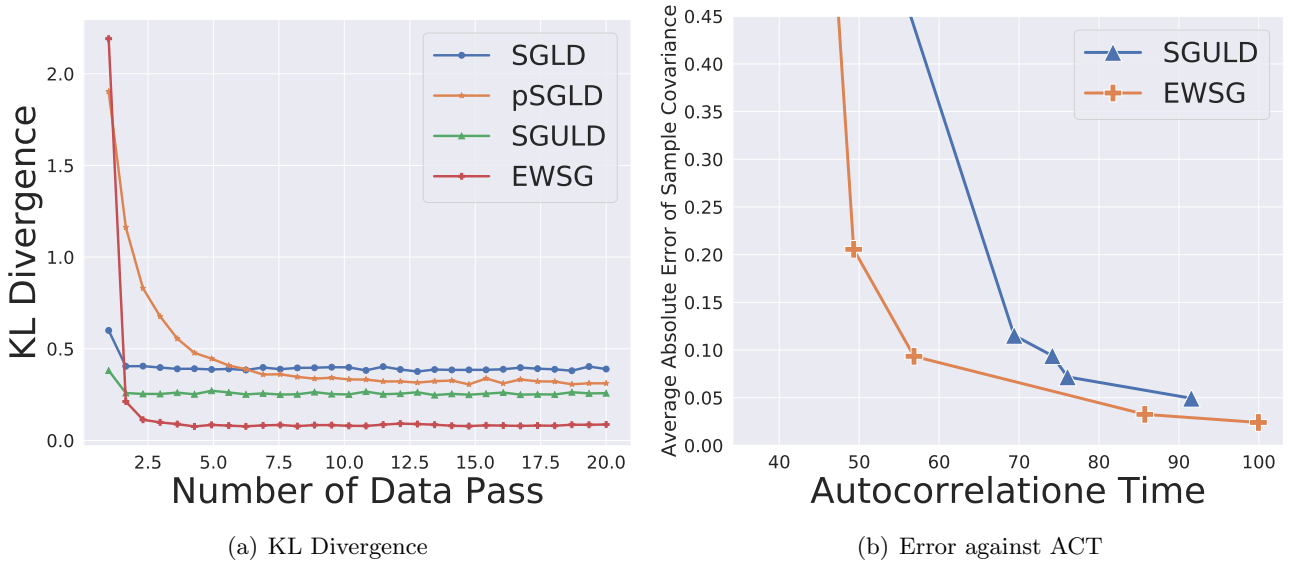


Figure 1: (a) Comparison of sample quality for SGLD, pSGLD, SGULD and EWSG in Kullback-Leibler divergence. (b) Average absolute error of sample covariance matrix against autocorrelation time plots of SGULD and EWSG.

5.2 A Misspecified Gaussian Case

In this subsection, we follow the same setup as in [3] and study a misspecified Gaussian model where one fits a one-dimensional normal distribution $p(\theta) = \mathcal{N}(\theta|\mu_0, \sigma_0^2)$ to 10^5 i.i.d points drawn according to $X_i \sim \log \mathcal{N}(0, 1)$, and flat prior is assigned $p(\mu_0, \log \sigma_0) \propto 1$. It was shown in [3] that FlyMC algorithm behaves erratically in this case, as ‘‘bright’’ data points with large values are rarely updated and they drive samples away from the target distribution. Consequently the chain mixes very slowly. One important commonality FlyMC shares with EWSG is that in each iteration, both algorithms select a subset of data in a non-uniform fashion. Therefore, it is interesting to investigate the performance of EWSG in this misspecified model.

For FlyMC³ used in this experiment, a tight lower bound based on Taylor’s expansion is used to minimize ‘‘bright’’ data points used per iteration. At each iteration, 10% data points are resampled and turned ‘‘on/off’’ accordingly and the step size is adaptively adjusted. FlyMC algorithm is run for 10000 iterations. Figure 2(a) shows the histogram of number of data points used in each iteration for FlyMC algorithm. On average, FlyMC consumes 10.9% of all data points per iteration. For fair

²Autocorrelation time is defined as $\tau = 1 + \sum_{s=0}^{\infty} \rho_s$, where ρ_s is the autocorrelation at time lag s .

³<https://github.com/rbardenet/2017JMLR-MCMCForTallData>

comparison, the minibatch size of EWSG is hence set $10^5 \times 10.9\% = 10900$ and we run EWSG for 1090 data passes. We set step size $h = 1 \times 10^{-4}$ and friction coefficient $\gamma = 300$ for EWSG. An isotropic random walk Metropolis Hasting (MH) is also run for sufficiently long and serves as the ground truth.

Figure 2(b) shows the autocorrelation of three algorithms. The autocorrelation of FlyMC decays very slowly, samples that are even 500 iterations away still show strong correlation. The autocorrelation of EWSG, on the other hand, decays much faster, suggesting EWSG explores parameter space more efficiently than FlyMC does. Figure 2(c) and 2(d) show the samples (the first 1000 samples are discarded as burn-in) generated by EWSG and FlyMC respectively. The samples of EWSG center around the mode of the target distribution while the samples of FlyMC are still far away from the true posterior. The experiment shows EWSG works quite well even in misspecified models, and hence is an effective candidate in combining importance sampling with scalable Bayesian inference.

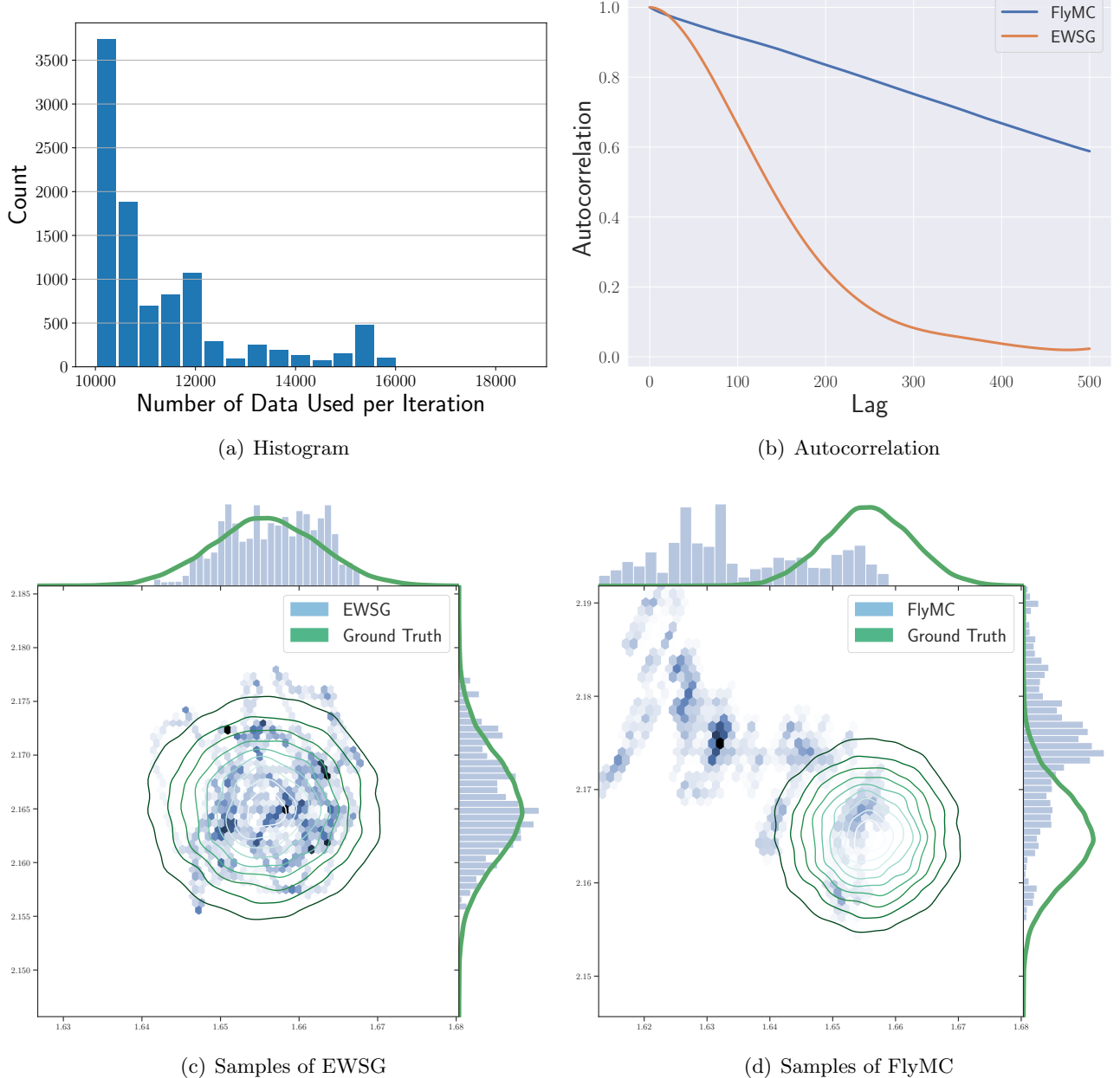


Figure 2: (a) Histogram of data used in each iteration for FlyMC algorithm. (b) Autocorrelation plot of FlyMC, EWSG and MH. (c) Samples of EWSG. (d) Samples of FlyMC.

5.3 Bayesian Logistic Regression

Consider Bayesian logistic regression for the binary classification problem. The probabilistic model for predicting a label y_k giving a feature vector x_k is $p(y_k = 1|x_k, \boldsymbol{\theta}) = 1/(1 + \exp(-\boldsymbol{\theta}^T \mathbf{x}_k))$. We set a

Gaussian prior with zero mean and covariance $\Sigma = 10I_d$ for parameter θ . We conduct our experiments on Covertype data set⁴, which contains 581,012 data points and 54 features. Given the large size of this data set, SG is needed to scale up MCMC methods. We use 80% of data for training and the rest 20% for testing.

The FlyMC algorithm⁵ use a lower bound derived in [22] for likelihood function. For underdamped Langevin based algorithms, we set friction coefficient $\gamma = 50$. After tuning, we set the step size as $\{1, 3, 0.02, 5, 5\} \times 10^{-3}$ for SGULD, EWSG, SGLD, pSGLD and FlyMC. All algorithms are run for one data pass, with minibatch size of 50 (for FlyMC, it means 50 data are sampled in each iteration to switch state). 20 independent samples are drawn from each algorithm to estimate statistics. To further smooth out noise, all experiments are repeated 10 times with different seeds.

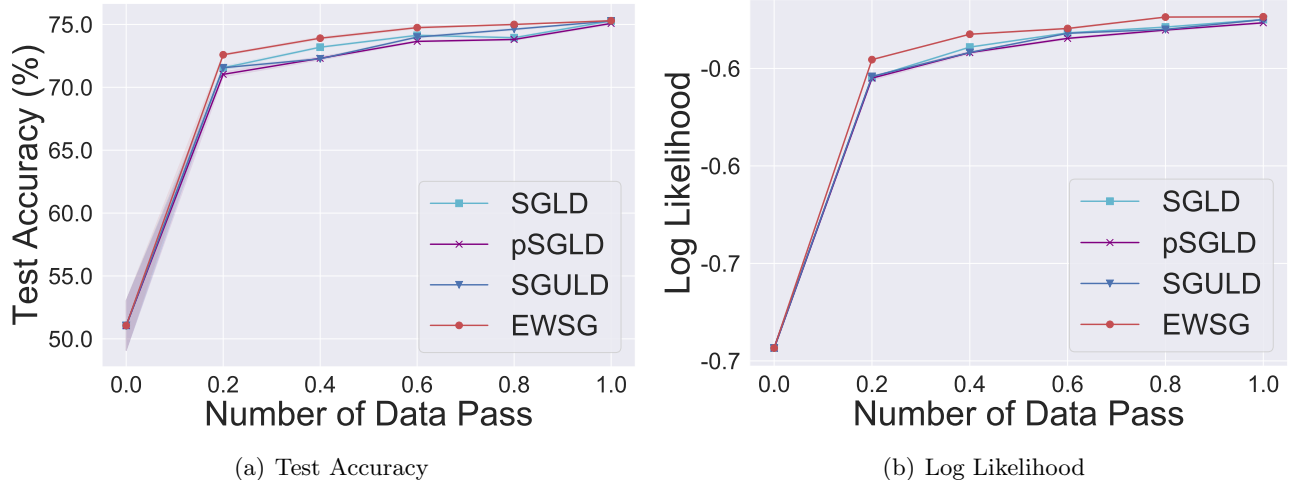


Figure 3: Learning curve of (a) accuracy, and (b) log likelihood on test data set. The shaded area denotes one standard deviation.

| Method | Accuracy(%) | Log Likelihood |
|--------|--|--|
| SGLD | 75.2823 ± 0.0788 | -0.5249 ± 0.0002 |
| pSGLD | 75.0785 ± 0.0939 | -0.5266 ± 0.0004 |
| SGULD | 75.2717 ± 0.0686 | -0.5250 ± 0.0001 |
| EWSG | 75.2928 ± 0.0452 | -0.5235 ± 0.0003 |
| FlyMC | 75.1650 ± 0.0792 | -0.5235 ± 0.0005 |

Table 1: Accuracy and log likelihood on test data set of all algorithms after one data pass, reported as mean \pm standard deviation format. The highest accuracy and the largest log likelihood are highlighted in boldface.

We plot learning curves in Fig. 3 and report final test accuracy and log likelihood on test set in Table 1. The final log likelihood of EWSG outperforms that of many competitors, and is comparable to FlyMC, known as an *exact* MCMC method. Moreover, EWSG achieves the best test accuracy.

5.4 Bayesian Neural Network

Bayesian inference is compelling for deep learning (see e.g. a recent review [34]) and here we apply our algorithm to Bayesian neural network (BNN)s. Two popular architecture of neural nets are experimented – multilayer perceptron (MLP) and convolutional neural nets (CNN). In MLP architecture, a hidden layer with 100 neurons followed by a softmax layer is used. In CNN, we use standard network configuration with 2 convolutional layers followed by 2 fully connected layers [16]. Both convolutional layers use 5×5 convolution kernel with 32 and 64 channels, 2×2 max pooling layers follow immediately after convolutional layer. The last two fully-connected layers each has 200 neurons. We set the standard normal as prior for all weights and bias.

⁴<https://archive.ics.uci.edu/ml/datasets/covtype>

⁵<https://github.com/HIPS/firefly-monte-carlo/tree/master/flymc>

We test algorithms on the MNIST data set, which consists of 60000 training data and 10000 test data, each datum is a 28×28 gray-scale image with one of the ten possible labels (digits 0 ~ 9). For underdamped Langevin based algorithms, we set friction coefficient $\gamma = 0.1$ in MLP and $\gamma = 1.0$ in CNN. In MLP, the step sizes are set $h = \{4, 2, 2\} \times 10^{-3}$ for EWSG, SGULD and CG-SGULD, and $h = \{0.001, 1\} \times 10^{-4}$ for SGLD and pSGLD, via grid search. For CP-SGULD (clustering-based preprocessing is conducted [15] before SGULD), we use Kmeans with 10 clusters to preprocess the data set. In CNN, the step sizes are set $h = \{4, 2, 2\} \times 10^{-3}$ for EWSG, SGULD and CG-SGULD, and $h = \{0.02, 8\} \times 10^{-6}$ for SGLD and pSGLD, via grid search. All algorithms use minibatch size of 100 and are run for 200 data passes. For each algorithm, we generate 10 independent samples to estimate posterior distributions and make prediction accordingly. To smooth out noise and obtain more significant results, we repeat all experiments 10 times with different seeds.

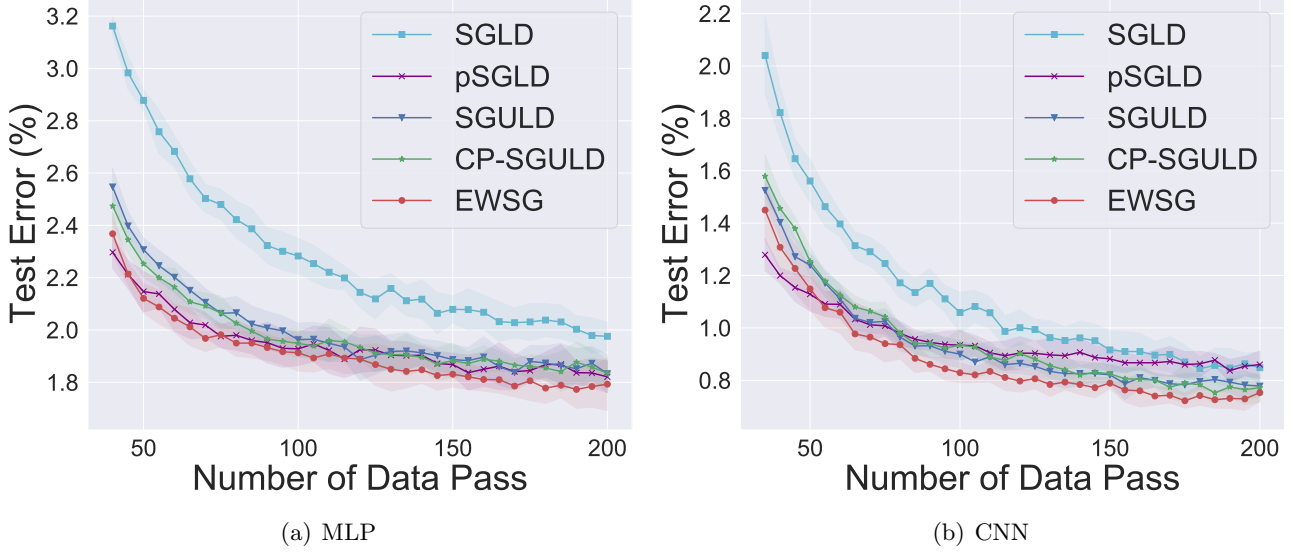


Figure 4: Test error on MNIST data set for (a) MLP and (b) CNN architecture. The shaded area denotes one standard deviation computed across 10 independent runs.

| Method | Test Error(%), MLP | Test Error(%), CNN |
|----------|-------------------------------------|-------------------------------------|
| SGLD | 1.976 ± 0.055 | 0.848 ± 0.060 |
| pSGLD | 1.821 ± 0.061 | 0.860 ± 0.052 |
| SGULD | 1.833 ± 0.073 | 0.778 ± 0.040 |
| CG-SGULD | 1.835 ± 0.047 | 0.772 ± 0.055 |
| EWSG | 1.793 ± 0.100 | 0.753 ± 0.035 |

Table 2: Test error (mean \pm standard deviation) after 200 epoches.

The learning curve and final test error are shown in Figure 4 and Table 2. We find EWSG consistently improve over its uniform gradient subsampling counterpart SGULD as well as CG-SGULD which is motivated by marrying importance sampling with SG-MCMC. Moreover, EWSG also outperforms two standard benchmarks SGLD and pSGLD.

In each iteration of EWSG, we run an index Markov chain of length M and select a “good” minibatch to estimate gradient, therefore EWSG essentially uses $b \times (M + 1)$ data points per iteration where b is minibatch size. How does EWSG compare with its uniform gradient subsampling counterpart with a larger minibatch size ($b \times (M + 1)$)?

We empirically answer this question in the context of BNN with MLP architecture. We use the same step size for SGULD and EWSG and experiment a large range of values of minibatch size b and index chain length M . Each algorithm is run for 200 data passes and 10 independent samples are drawn to estimate test error. The results are shown in Table 3. We find that EWSG beats SGULD with larger minibatch in 8 out of 9 comparison groups, which suggests in general EWSG could be a better way to consuming data compared to increasing minibatch size and may shed light on other areas where stochastic gradient methods are used (e.g. optimization).

| b | $M + 1 = 2$ | $M + 1 = 5$ | $M + 1 = 10$ |
|-----|-----------------------|-----------------------|-----------------------|
| 100 | 1.86% 1.94% | 1.83% 1.92% | 1.80% 1.97% |
| 200 | 1.90% 1.87% | 1.87% 1.97% | 1.80% 2.07% |
| 500 | 1.79% 1.97% | 2.01% 2.17% | 2.36% 2.37% |

Table 3: Test errors of **EWSG** (top of each cell) and **SGULD** (bottom of each cell) after 200 epoches. b is minibatch size for **EWSG**, and minibatch size of **SGULD** is set as $b \times (M + 1)$ to ensure the same number of data used per parameter update for both algorithms. Step size is set $h = \frac{10}{b(M+1)}$ as suggested in [10], different from that used to produce Table 2. Results with smaller test error is highlighted in boldface.

6 Conclusion

In this paper, we proposed EWSG, which uses exponentially weighted subsampling of gradients to match the transition kernel of a base MCMC base with full gradient. The goal is better sample quality. Both local variance analysis and global non-asymptotic analysis are presented to demonstrate the advantage of EWSG theoretically. Empirical results also showed improved sampling/learning performance. We believe non-uniform stochastic gradient can be introduced to a large class of MCMC methods and capable for impactful algorithmic improvements.

AAcknowledgement

The authors thank Wenlong Mou for discussions. MT was partially supported by NSF DMS-1847802 and ECCS-1936776.

References

- [1] Sungjin Ahn, Anoop Korattikara, and Max Welling. Bayesian posterior sampling via stochastic gradient fisher scoring. In *29th International Conference on Machine Learning, ICML 2012*, pages 1591–1598, 2012.
- [2] Francis Bach. Stochastic gradient methods for machine learning. Technical report, 2013.
- [3] Rémi Bardenet, Arnaud Doucet, and Chris Holmes. On markov chain monte carlo methods for tall data. *The Journal of Machine Learning Research*, 18(1):1515–1557, 2017.
- [4] Vivek S Borkar and Sanjoy K Mitter. A strong approximation theorem for stochastic recursive algorithms. *Journal of optimization theory and applications*, 100(3):499–513, 1999.
- [5] Nawaf Bou-Rabee, Andreas Eberle, and Raphael Zimmer. Coupling and convergence for Hamiltonian Monte Carlo. *arXiv preprint arXiv:1805.00452*, 2018.
- [6] Nawaf Bou-Rabee and Houman Owhadi. Long-run accuracy of variational integrators in the stochastic context. *SIAM Journal on Numerical Analysis*, 48(1):278–297, 2010.
- [7] Nawaf Bou-Rabee and Jesús María Sanz-Serna. Geometric integrators and the Hamiltonian Monte Carlo method. *Acta Numerica*, 27:113–206, 2018.
- [8] Steve Brooks, Andrew Gelman, Galin Jones, and Xiao-Li Meng. *Handbook of markov chain monte carlo*. CRC press, 2011.

[9] Changyou Chen, Nan Ding, and Lawrence Carin. On the convergence of stochastic gradient mcmc algorithms with high-order integrators. In *Advances in Neural Information Processing Systems*, pages 2278–2286, 2015.

[10] Tianqi Chen, Emily B Fox, and Carlos Guestrin. Stochastic Gradient Hamiltonian Monte Carlo. *International Conference on Machine Learning*, pages 1683–1691, 2014.

[11] Xiang Cheng, Niladri S Chatterji, Yasin Abbasi-Yadkori, Peter L Bartlett, and Michael I Jordan. Sharp convergence rates for langevin dynamics in the nonconvex setting. *arXiv preprint arXiv:1805.01648*, 2018.

[12] Xiang Cheng, Niladri S Chatterji, Peter L Bartlett, and Michael I Jordan. Underdamped langevin mcmc: A non-asymptotic analysis. *Proceedings of the 31st Conference On Learning Theory, PMLR*, 2018.

[13] Dominik Csiba and Peter Richtárik. Importance sampling for minibatches. *The Journal of Machine Learning Research*, 19(1):962–982, 2018.

[14] Kumar Avinava Dubey, Sashank J Reddi, Sinead A Williamson, Barnabas Poczos, Alexander J Smola, and Eric P Xing. Variance reduction in stochastic gradient langevin dynamics. In *Advances in neural information processing systems*, pages 1154–1162, 2016.

[15] Tianfan Fu and Zhihua Zhang. Cpsg-mcmc: Clustering-based preprocessing method for stochastic gradient mcmc. In *Artificial Intelligence and Statistics*, pages 841–850, 2017.

[16] Kevin Jarrett, Koray Kavukcuoglu, Marc’Aurelio Ranzato, and Yann LeCun. What is the best multi-stage architecture for object recognition? In *2009 IEEE 12th international conference on computer vision*, pages 2146–2153. IEEE, 2009.

[17] Rie Johnson and Tong Zhang. Accelerating stochastic gradient descent using predictive variance reduction. In *Advances in neural information processing systems*, pages 315–323, 2013.

[18] Rep Kubo. The fluctuation-dissipation theorem. *Reports on progress in physics*, 29(1):255, 1966.

[19] Chunyuan Li, Changyou Chen, David Carlson, and Lawrence Carin. Preconditioned stochastic gradient langevin dynamics for deep neural networks. In *Thirtieth AAAI Conference on Artificial Intelligence*, 2016.

[20] Qianxiao Li, Cheng Tai, and E Weinan. Stochastic modified equations and adaptive stochastic gradient algorithms. In *International Conference on Machine Learning*, pages 2101–2110, 2017.

[21] Moshe Lichman et al. UCI machine learning repository, 2013.

[22] Dougal Maclaurin and Ryan Prescott Adams. Firefly monte carlo: Exact mcmc with subsets of data. In *Twenty-Fourth International Joint Conference on Artificial Intelligence*, 2015.

[23] Stephan Mandt, Matthew D Hoffman, and David M Blei. Stochastic gradient descent as approximate bayesian inference. *The Journal of Machine Learning Research*, 18(1):4873–4907, 2017.

[24] Jonathan C Mattingly, Andrew M Stuart, and Michael V Tretyakov. Convergence of numerical time-averaging and stationary measures via poisson equations. *SIAM Journal on Numerical Analysis*, 48(2):552–577, 2010.

[25] Deanna Needell, Rachel Ward, and Nati Srebro. Stochastic gradient descent, weighted sampling, and the randomized kaczmarz algorithm. In *Advances in Neural Information Processing Systems*, pages 1017–1025, 2014.

[26] Sam Patterson and Yee Whye Teh. Stochastic gradient Riemannian Langevin dynamics on the probability simplex. *Advances in Neural Information Processing Systems*, pages 3102–3110, 2013.

- [27] Grigoris A Pavliotis. *Stochastic processes and applications: diffusion processes, the Fokker-Planck and Langevin equations*, volume 60. Springer, 2014.
- [28] Gareth O Roberts, Richard L Tweedie, et al. Exponential convergence of langevin distributions and their discrete approximations. *Bernoulli*, 2(4):341–363, 1996.
- [29] Mark Schmidt, Reza Babanezhad, Mohamed Ahmed, Aaron Defazio, Ann Clifton, and Anoop Sarkar. Non-uniform stochastic average gradient method for training conditional random fields. In *artificial intelligence and statistics*, pages 819–828, 2015.
- [30] Mark Schmidt, Nicolas Le Roux, and Francis Bach. Minimizing finite sums with the stochastic average gradient. *Mathematical Programming*, 162(1-2):83–112, 2017.
- [31] Yee Whye Teh, Alexandre H Thiery, and Sebastian J Vollmer. Consistency and fluctuations for stochastic gradient langevin dynamics. *The Journal of Machine Learning Research*, 17(1):193–225, 2016.
- [32] Sebastian J Vollmer, Konstantinos C Zygalakis, and Yee Whye Teh. Exploration of the (non-) asymptotic bias and variance of stochastic gradient langevin dynamics. *The Journal of Machine Learning Research*, 17(1):5504–5548, 2016.
- [33] Max Welling and Yee Whye Teh. Bayesian learning via stochastic gradient langevin dynamics. *International Conference on Machine Learning*, pages 681–688, 2011.
- [34] Andrew Gordon Wilson. The case for bayesian deep learning. *arXiv preprint arXiv:2001.10995*, 2020.
- [35] Peilin Zhao and Tong Zhang. Stochastic optimization with importance sampling for regularized loss minimization. In *International Conference on Machine Learning*, pages 1–9, 2015.
- [36] Rong Zhu. Gradient-based sampling: An adaptive importance sampling for least-squares. In *Advances in Neural Information Processing Systems*, pages 406–414, 2016.

A Proof of Theorem 1

Proof: Denote the set of all n -dimensional probability vectors by Σ^n , the set of sparse probability vectors by \mathcal{S} , and the set of non-sparse (dense) probability vectors by $\mathcal{D} = \Sigma^n \setminus \mathcal{S}$. Denote $B = [\mathbf{b}_1, \dots, \mathbf{b}_n]$, then the optimization problem can be written as

$$\begin{aligned} & \min \sum_{i=1}^n p_i \|\mathbf{b}_i\|^2 \\ \text{s.t. } & \begin{cases} B\mathbf{p} = \mathbf{0} \\ \mathbf{p}^T \mathbf{1}_n = 1 \\ p_i \geq 0, i = 1, 2, \dots, n \end{cases} \end{aligned}$$

Note that the feasible region is always non-empty (take \mathbf{p} to be a uniform distribution) and is also closed and bounded, hence this linear programming is always solvable. Denote the set of all minimizers by \mathcal{M} . Note that \mathcal{M} depends on $\mathbf{b}_1, \dots, \mathbf{b}_n$ and is in this sense random.

The Lagrange function is

$$L(\mathbf{p}, \boldsymbol{\lambda}, \mu, \boldsymbol{\omega}) = \mathbf{p}^T \mathbf{s} - \boldsymbol{\lambda}^T B\mathbf{p} - \mu(\mathbf{p}^T \mathbf{1}_n) - \boldsymbol{\omega}^T \mathbf{p}$$

where $\mathbf{s} = [\|\mathbf{b}_1\|^2, \|\mathbf{b}_2\|^2, \dots, \|\mathbf{b}_n\|^2]^T$ and $\boldsymbol{\lambda}, \mu, \boldsymbol{\omega}$ are dual variables. The optimality condition reads as

$$\frac{\partial L}{\partial \mathbf{p}} = \mathbf{s} - B^T \boldsymbol{\lambda} - \mu \mathbf{1}_n - \boldsymbol{\omega} = \mathbf{0}$$

Dual feasibility and complementary slackness require

$$\begin{aligned} \omega_i &\leq 0, i = 1, 2, \dots, n \\ \boldsymbol{\omega}^T \mathbf{p} &= 0 \end{aligned}$$

Consider the probability of the event $\{\text{a dense probability vector can solve the above minimization problem}\}$, i.e., $\mathbb{P}(\mathcal{M} \cap \mathcal{D} \neq \emptyset)$. It is upper bounded by

$$\mathbb{P}(\mathcal{M} \cap \mathcal{D} \neq \emptyset) \leq \mathbb{P}(\mathbf{p} \in \mathcal{D} \text{ and } \mathbf{p} \text{ solves KKT condition})$$

Since $\mathbf{p} \in \mathcal{D}$, complementary slackness implies that at least $d+2$ entries in $\boldsymbol{\omega}$ are zero. Denote the indices of these entries by \mathcal{J} . For every $j \in \mathcal{J}$, by optimality condition, we have $s_j - \boldsymbol{\lambda}^T \mathbf{b}_j - \mu = 0$, i.e.,

$$\|\mathbf{b}_j\|^2 - \boldsymbol{\lambda}^T \mathbf{b}_j - \mu = 0$$

Take the first $d+1$ indices in \mathcal{J} , and note a geometric fact that $d+1$ points in a d -dimensional space must be on the surface of a hypersphere of at most $d-1$ dimension, which we denote by $\mathcal{S} = S^{q-1} + \mathbf{x}$ for some vector \mathbf{x} and integer $q \leq d$. Because b_i 's distribution is absolutely continuous, we have

$$\begin{aligned} & \mathbb{P}(\mathbf{p} \in \mathcal{D} \text{ and } \mathbf{p} \text{ solves KKT condition}) \\ & \leq \mathbb{P}(\mathbf{p} \in \mathcal{D} \text{ and } \mathbf{b}_j \in \mathcal{S}, \forall j \in \mathcal{J}) \\ & \leq \mathbb{P}(\mathbf{b}_j \in \mathcal{S}, \forall j \in \mathcal{J}) \\ & = \mathbb{P}(\mathbf{b}_{j_k} \in \mathcal{S}, k = d+2, \dots, |\mathcal{J}|) \\ & = \prod_{k=d+2}^{|\mathcal{J}|} \mathbb{P}(\mathbf{b}_{j_k} \in \mathcal{S}) \quad (\text{independence}) \\ & = 0 \quad (\text{absolute continuous}) \end{aligned}$$

Hence $\mathbb{P}(\mathcal{M} \cap \mathcal{D} \neq \emptyset) = 0$ and

$$\begin{aligned} 1 &= \mathbb{P}(\mathcal{M} \neq \emptyset) \\ &= \mathbb{P}((\mathcal{M} \cap \mathcal{S}) \cup (\mathcal{M} \cap \mathcal{D}) \neq \emptyset) \\ &\leq \mathbb{P}(\mathcal{M} \cap \mathcal{S} \neq \emptyset) + \mathbb{P}(\mathcal{M} \cap \mathcal{D} \neq \emptyset) \\ &= \mathbb{P}(\mathcal{M} \cap \mathcal{S} \neq \emptyset) \end{aligned}$$

Therefore we have

$$\mathbb{P}(\mathcal{M} \cap \mathcal{S} \neq \emptyset) = 1$$

■

B Proof of Theorem 2

Proof: The transition kernel of EM discretization with full gradient can be explicitly written as

$$\begin{aligned} & P^{EM}(\boldsymbol{\theta}_{k+1}, \mathbf{r}_{k+1} | \boldsymbol{\theta}_k, \mathbf{r}_k) \\ &= \delta(\boldsymbol{\theta}_{k+1} - (\boldsymbol{\theta}_k + \mathbf{r}_k h)) \\ & \quad \times \Phi\left(\frac{\mathbf{r}_{k+1} - \mathbf{r}_k + h\gamma \mathbf{r}_k + h\nabla V(\boldsymbol{\theta}_k)}{\sigma\sqrt{h}}\right) \frac{1}{\sigma\sqrt{h}} \end{aligned}$$

where $\delta(\cdot)$ is the Dirac delta function and $\Phi(\cdot)$ is the probability density of d -dimensional standard normal distribution.

Denote the unnormalized probability measure of index I_k by

$$\tilde{p}_i = \exp\left\{-\frac{\|\mathbf{x} + \sum_{j=1}^n \mathbf{a}_j\|^2}{2} + \frac{\|\mathbf{x} + n\mathbf{a}_i\|^2}{2}\right\}$$

and the normalization constant by

$$\hat{Z} = \sum_{i=1}^n \int \tilde{p}_i d\mathbf{r}_{k+1}.$$

Then the transition kernel of EWSG can be written as

$$\begin{aligned} & \tilde{P}^{EM}(\boldsymbol{\theta}_{k+1}, \mathbf{r}_{k+1} | \boldsymbol{\theta}_k, \mathbf{r}_k) \\ &= \delta(\boldsymbol{\theta}_{k+1} - (\boldsymbol{\theta}_k + \mathbf{r}_k h)) \sum_{i=1}^n p_i \Phi\left(\frac{\mathbf{r}_{k+1} - \mathbf{r}_k + h\gamma \mathbf{r}_k + hn\nabla V_i(\boldsymbol{\theta}_k)}{\sigma\sqrt{h}}\right) \frac{1}{\sigma\sqrt{h}} \\ &= \delta(\boldsymbol{\theta}_{k+1} - (\boldsymbol{\theta}_k + \mathbf{r}_k h)) \sum_{i=1}^n \frac{\tilde{p}_i}{\hat{Z}} \Phi\left(\frac{\mathbf{r}_{k+1} - \mathbf{r}_k + h\gamma \mathbf{r}_k + hn\nabla V_i(\boldsymbol{\theta}_k)}{\sigma\sqrt{h}}\right) \frac{1}{\sigma\sqrt{h}} \\ &= \frac{1}{\hat{Z}} \delta(\boldsymbol{\theta}_{k+1} - (\boldsymbol{\theta}_k + \mathbf{r}_k h)) \sum_{i=1}^n \exp\left\{-\frac{\|\mathbf{x} + \sum_{j=1}^n \mathbf{a}_j\|^2}{2} + \frac{\|\mathbf{x} + n\mathbf{a}_i\|^2}{2}\right\} \frac{1}{\sqrt{(2\pi)^d}} \exp\left\{-\frac{\|\mathbf{x} + n\mathbf{a}_i\|^2}{2}\right\} \frac{1}{\sigma\sqrt{h}} \\ &= \frac{n}{\hat{Z}\sqrt{(2\pi)^d}} \delta(\boldsymbol{\theta}_{k+1} - (\boldsymbol{\theta}_k + \mathbf{r}_k h)) \exp\left\{-\frac{\|\mathbf{x} + \sum_{j=1}^n \mathbf{a}_j\|^2}{2}\right\} \frac{1}{\sigma\sqrt{h}} \end{aligned}$$

Recall the transition kernel of EM integrator with full gradient is

$$\begin{aligned} P^{EM}(\boldsymbol{\theta}_{k+1}, \mathbf{r}_{k+1} | \boldsymbol{\theta}_k, \mathbf{r}_k) &= \delta(\boldsymbol{\theta}_{k+1} - (\boldsymbol{\theta}_k + \mathbf{r}_k h)) \Phi\left(\frac{\mathbf{r}_{k+1} - \mathbf{r}_k + h\gamma \mathbf{r}_k + h\nabla V(\boldsymbol{\theta}_k)}{\sigma\sqrt{h}}\right) \frac{1}{\sigma\sqrt{h}} \\ &= \delta(\boldsymbol{\theta}_{k+1} - (\boldsymbol{\theta}_k + \mathbf{r}_k h)) \frac{1}{\sqrt{(2\pi)^d}} \exp\left\{-\frac{\|\mathbf{x} + \sum_{j=1}^n \mathbf{a}_j\|^2}{2}\right\} \frac{1}{\sigma\sqrt{h}} \end{aligned}$$

As both transition kernels are proportional to

$$\delta(\boldsymbol{\theta}_{k+1} - (\boldsymbol{\theta}_k + \mathbf{r}_k h)) \exp\left\{-\frac{\|\mathbf{x} + \sum_{j=1}^n \mathbf{a}_j\|^2}{2}\right\}$$

We therefore conclude that

$$P^{EM}(\boldsymbol{\theta}_{k+1}, \mathbf{r}_{k+1} | \boldsymbol{\theta}_k, \mathbf{r}_k) = \tilde{P}^{EM}(\boldsymbol{\theta}_{k+1}, \mathbf{r}_{k+1} | \boldsymbol{\theta}_k, \mathbf{r}_k)$$

■

C Proof of Theorem 3

Proof: Let $\mathbf{b}_i = n\nabla V_i$ and assume $\|\mathbf{b}_i\|_2 \leq R$ for some constant R . Denote $B = [\mathbf{b}_1, \mathbf{b}_2, \dots, \mathbf{b}_n]$. For any probability distribution \mathbf{p} over $\{1, \dots, n\}$, we have

$$\begin{aligned} & \text{cov}_{I \sim \mathbf{p}}[\mathbf{b}_I | \mathbf{b}_1, \dots, \mathbf{b}_n] \\ &= \sum_{i=1}^n p_i \mathbf{b}_i \mathbf{b}_i^T - \left(\sum_{i=1}^n p_i \mathbf{b}_i \right) \left(\sum_{i=1}^n p_i \mathbf{b}_i \right)^T \\ &= \sum_{i=1}^n p_i \mathbf{b}_i \mathbf{b}_i^T \sum_{i=1}^n p_i - \left(\sum_{i=1}^n p_i \mathbf{b}_i \right) \left(\sum_{i=1}^n p_i \mathbf{b}_i \right)^T \\ &= \sum_{i < j} (\mathbf{b}_i - \mathbf{b}_j)(\mathbf{b}_i - \mathbf{b}_j)^T p_i p_j \end{aligned}$$

Therefore we let

$$\begin{aligned} f(B) &:= \text{Tr} \left[\sum_{i < j} (\mathbf{b}_i - \mathbf{b}_j)(\mathbf{b}_i - \mathbf{b}_j)^T p_i p_j - \sum_{i < j} (\mathbf{b}_i - \mathbf{b}_j)(\mathbf{b}_i - \mathbf{b}_j)^T \frac{1}{n^2} \right] \\ &= \sum_{i < j} \|\mathbf{b}_i - \mathbf{b}_j\|^2 p_i p_j - \sum_{i < j} \|\mathbf{b}_i - \mathbf{b}_j\|^2 \frac{1}{n^2} \quad (\text{Tr}[AB] = \text{Tr}[BA]) \end{aligned}$$

and use it to compare the trace of covariance matrix of uniform- and nonuniform- subsamplings.

First of all,

$$\begin{aligned} & \mathbb{E}[f(B)] \\ &= \mathbb{E}[\|\mathbf{b}_i - \mathbf{b}_j\|^2] \sum_{i < j} \left(p_i p_j - \frac{1}{n^2} \right) \\ &= \mathbb{E}[\|\mathbf{b}_i - \mathbf{b}_j\|^2] \left(\sum_{i < j} p_i p_j - \frac{n-1}{2n} \right) \\ &= \mathbb{E}[\|\mathbf{b}_i - \mathbf{b}_j\|^2] \left(\frac{1 - \sum_{i=1}^n p_i^2}{2} - \frac{n-1}{2n} \right) \\ &\leq \mathbb{E}[\|\mathbf{b}_i - \mathbf{b}_j\|^2] \left(\frac{1 - \frac{1}{n}}{2} - \frac{n-1}{2n} \right) \\ &= 0 \end{aligned}$$

where the inequality is due to Cauchy-Schwarz and it is a strict inequality unless all p_i 's are equal, which means uniform subsampling on average has larger variability than a non-uniform scheme measured by the trace of covariance matrix.

Moreover, concentration inequality can help show $f(B)$ is negative with high probability if h is small. To this end, plug $\mathbf{x} = \mathcal{O}(\sqrt{h})$ in and rewrite

$$p_i = \frac{1}{Z} \exp \left\{ Fh \left[\frac{\|\mathbf{y} + \frac{1}{n} \sum_{i=1}^n \mathbf{b}_i\|^2}{2} - \frac{\|\mathbf{y} + \mathbf{b}_i\|^2}{2} \right] \right\}$$

where $\mathbf{y} = \frac{\sigma}{\sqrt{h}} \mathbf{x} = \mathcal{O}(1)$, $F = -\frac{1}{\sigma^2}$ and Z is the normalization constant. Denote the unnormalized probability by

$$\tilde{p}_i = \exp \left\{ Fh \left[\frac{\|\mathbf{y} + \frac{1}{n} \sum_{i=1}^n \mathbf{b}_i\|^2}{2} - \frac{\|\mathbf{y} + \mathbf{b}_i\|^2}{2} \right] \right\}$$

and we have

$$\begin{aligned} f(B) &= \frac{1}{2} \sum_{i=1}^n \sum_{j=1}^n \|\mathbf{b}_i - \mathbf{b}_j\|^2 \left(p_i p_j - \frac{1}{n^2} \right) \\ &= \frac{1}{2} \sum_{i=1}^n \sum_{j=1}^n \|\mathbf{b}_i - \mathbf{b}_j\|^2 \frac{\tilde{p}_i \tilde{p}_j}{[\sum_{k=1}^n \tilde{p}_k]^2} - \frac{1}{2} \sum_{i=1}^n \sum_{j=1}^n \|\mathbf{b}_i - \mathbf{b}_j\|^2 \frac{1}{n^2} \end{aligned}$$

To prove concentration results, it is useful to estimate

$$\begin{aligned} C_i &= \sup_{\substack{\mathbf{b}_1, \dots, \mathbf{b}_n \in B(\mathbf{0}, R) \\ \hat{\mathbf{b}}_i \in B(\mathbf{0}, R)}} |f(\mathbf{b}_1, \dots, \mathbf{b}_i, \dots, \mathbf{b}_n) \\ &\quad - f(\mathbf{b}_1, \dots, \hat{\mathbf{b}}_i, \dots, \mathbf{b}_n)| \end{aligned}$$

where $B(\mathbf{0}, R)$ is a ball centered at origin with radius R in \mathbb{R}^d .

Due to the mean value theorem, we have $C_i \leq 2R \sup |\frac{\partial f}{\partial \mathbf{b}_i}|$. By symmetry, it suffices to compute $\sup |\frac{\partial f}{\partial \mathbf{b}_1}|$ to upper bound C_1 . Note that

$$\frac{\partial \tilde{p}_j}{\partial \mathbf{b}_1} = 2\tilde{p}_j Fh \left[\frac{1}{n} (\mathbf{y} + \frac{1}{n} \sum_{i=1}^n \mathbf{b}_i) - (\mathbf{y} + \mathbf{b}_j) \delta_{1j} \right] = \mathcal{O}(h) \tilde{p}_j$$

where δ_{1j} is the Kronecker delta function. Thus

$$\begin{aligned} \frac{\partial f}{\partial \mathbf{b}_1} &= \sum_{j=1}^n (\mathbf{b}_1 - \mathbf{b}_j) \frac{\tilde{p}_1 \tilde{p}_j}{[\sum_{k=1}^n \tilde{p}_k]^2} - \sum_{j=1}^n (\mathbf{b}_1 - \mathbf{b}_j) \frac{1}{n^2} + \sum_{i,j=1}^n \|\mathbf{b}_1 - \mathbf{b}_j\|^2 \frac{\mathcal{O}(h) \tilde{p}_i \tilde{p}_j}{[\sum_{k=1}^n \tilde{p}_k]^2} \\ &\quad - 2 \sum_{i,j=1}^n \|\mathbf{b}_1 - \mathbf{b}_j\|^2 \frac{\tilde{p}_i \tilde{p}_j}{[\sum_{k=1}^n \tilde{p}_k]^3} \sum_{k=1}^n \tilde{p}_k \mathcal{O}(h) \\ &= \tilde{p}_1 \sum_{j=1}^n (\mathbf{b}_1 - \mathbf{b}_j) \frac{\tilde{p}_j}{[\sum_{k=1}^n \tilde{p}_k]^2} - \sum_{j=1}^n (\mathbf{b}_1 - \mathbf{b}_j) \frac{1}{n^2} + \frac{\mathcal{O}(n^2) \mathcal{O}(h)}{\mathcal{O}(n^2)} + \frac{\mathcal{O}(n^2)}{\mathcal{O}(n^3)} \mathcal{O}(n) \mathcal{O}(h) \\ &= \mathcal{O}\left(\frac{h}{n}\right) + \mathcal{O}(h) + \mathcal{O}(h) \\ &= \mathcal{O}(h) \end{aligned}$$

where $\mathcal{O}(\frac{h}{n})$ in the 2nd last equation comes from the difference of the first two terms in the 3rd last equation. This estimation shows that $C_i \leq 2R\mathcal{O}(h) = \mathcal{O}(h)$.

Therefore, by McDiarmid's inequality, we conclude for any $\epsilon > 0$,

$$\mathbb{P}(|f - \mathbb{E}[f]| > \epsilon) \leq 2 \exp \left(\frac{-2\epsilon^2}{\sum_{i=1}^n C_i^2} \right) = 2 \exp \left(\frac{-2\epsilon^2}{n\mathcal{O}(h^2)} \right).$$

Any choice of $h(n) = o(n^{-1/2})$ will render this probability asymptotically vanishing as n grows, which means that f will be negative with high probability, which is equivalent to reduced variance per step. ■

D Proof of Theorem 4

Proof: We rewrite the generator of underdamped Langevin with full gradient as

$$\mathcal{L}f(\mathbf{X}) = \mathbf{F}(\mathbf{X})^T \begin{bmatrix} \nabla_{\boldsymbol{\theta}} f(\mathbf{X}) \\ \nabla_{\mathbf{r}} f(\mathbf{X}) \end{bmatrix} + \frac{1}{2} A : \nabla \nabla f(\mathbf{X})$$

where

$$\mathbf{F}(\mathbf{X}) = \begin{bmatrix} \mathbf{r} \\ -\gamma \mathbf{r} - \nabla V(\boldsymbol{\theta}) \end{bmatrix}, \quad A = GG^T \text{ and } G = \begin{bmatrix} O_{d \times d} & O_{d \times d} \\ O_{d \times d} & \sqrt{2\gamma} I_{d \times d} \end{bmatrix}$$

Rewrite the discretized underdamped Langevin with stochastic gradient in variable \mathbf{X}

$$\mathbf{X}_{k+1}^E - \mathbf{X}_k^E = h\mathbf{F}_k(\mathbf{X}_k^E) + \sqrt{h}G_k\boldsymbol{\eta}_{k+1}$$

where

$$\mathbf{F}_k(\mathbf{X}) = \begin{bmatrix} \mathbf{r} \\ -\gamma\mathbf{r} - n\nabla V_{I_k}(\boldsymbol{\theta}) \end{bmatrix}, \quad G_k = G = \begin{bmatrix} O_{d \times d} & O_{d \times d} \\ O_{d \times d} & \sqrt{2\gamma}I_{d \times d} \end{bmatrix}$$

and $\boldsymbol{\eta}_{k+1}$ is a $2d$ dimensional standard Gaussian random vector. Note that this representation include both SGULD and EWSG, for SGULD I_k follows uniform distribution and for EWSG, I_k follows the MCMC-approximated exponentially weighted distribution.

Denote the generator associated with stochastic gradient underdamped Langevin at the k -th iteration by

$$\mathcal{L}_k f(\mathbf{X}) = \mathbf{F}_k(\mathbf{X})^T \begin{bmatrix} \nabla_{\boldsymbol{\theta}} f(\mathbf{X}) \\ \nabla_{\mathbf{r}} f(\mathbf{X}) \end{bmatrix} + \frac{1}{2}A : \nabla \nabla f(\mathbf{X})$$

and the difference of the generators of full gradient and stochastic gradient underdamped Langevin at k -th iteration is denoted by

$$\Delta \mathcal{L}_k f(\mathbf{X}) = (\mathcal{L}_k - \mathcal{L}) f(\mathbf{X}) = (\mathbf{F}_k(\mathbf{X}) - \mathbf{F}(\mathbf{X}))^T \begin{bmatrix} \nabla_{\boldsymbol{\theta}} f(\mathbf{X}) \\ \nabla_{\mathbf{r}} f(\mathbf{X}) \end{bmatrix} = \langle \nabla V(\boldsymbol{\theta}) - n\nabla V_{I_k}(\boldsymbol{\theta}), \nabla_{\mathbf{r}} f(\mathbf{X}) \rangle$$

For brevity, we write $\phi_k = \phi(\mathbf{X}_k^E)$, $\mathbf{F}_k^E = \mathbf{F}_k(\mathbf{X}_k^E)$, $\psi_k = \psi(\mathbf{X}_k^E)$ and $D^l \phi_k = (D^l \psi)(\mathbf{X}_k^E)$ where $(D^l \psi)(z)$ is the l -th order derivative. We write $(D^l \psi)[\mathbf{s}_1, \mathbf{s}_2, \dots, \mathbf{s}_l]$ for derivative evaluated in the direction $\mathbf{s}_j, j = 1, 2, \dots, l$. Define

$$\boldsymbol{\delta}_k = \mathbf{X}_{k+1}^E - \mathbf{X}_k^E = h\mathbf{F}_k^E + \sqrt{h}G_k\boldsymbol{\eta}_{k+1}$$

Under Assumption 1 and 2, we show that the vector field \mathbf{F}_k^E also has bounded momentum up to p -th order.

Lemma 5 *Under Assumption 1 and 2, there exists a constant M such that up to p -th order moments of random vector field \mathbf{F}_k^E are bounded*

$$\mathbb{E} \|\mathbf{F}_k^E\|_2^j \leq M, \forall j = 0, 1, 2, \dots, p, \forall k = 0, 1, 2, \dots,$$

Proof: It suffices to bound the highest moment, as all other lower order moments are bounded by the highest one by Holder's inequality.

First notice that

$$\|\mathbf{F}_k^E\|_2 = \left\| \begin{bmatrix} \mathbf{r}_k^E \\ -\gamma\mathbf{r}_k^E - \nabla V_{I_k}(\boldsymbol{\theta}_k^E) \end{bmatrix} \right\|_2 \leq \sqrt{1 + \gamma^2} \|\mathbf{r}_k^E\|_2 + \|\nabla V_{I_k}(\boldsymbol{\theta}_k^E)\|_2 \leq \sqrt{1 + \gamma^2} \|\mathbf{r}_k^E\|_2 + M_1$$

Hence

$$\begin{aligned} \mathbb{E} \|\mathbf{F}_k^E\|_2^p &\leq \mathbb{E} \left(\sqrt{1 + \gamma^2} \|\mathbf{r}_k^E\|_2 + M_1 \right)^p \\ &= \mathbb{E} \left\{ \sum_{i=0}^p \binom{p}{i} \|\mathbf{r}_k^E\|_2^i M_1^{p-i} \right\} \\ &= \sum_{i=0}^p \binom{p}{i} M_1^{p-i} \mathbb{E} \|\mathbf{r}_k^E\|_2^i \end{aligned}$$

By Assumption 2, we know each $\mathbb{E} \|\mathbf{r}_k^E\|_2^i, i = 0, 1, \dots, p$ is bounded, so we conclude there exists a constant $M > 0$ that bounds the p -th order moment of $\mathbf{F}_k^E, \forall k = 0, 1, \dots$ ■

Using Taylor's expansion for ψ , we have

$$\psi_{k+1} = \psi_k + D\psi_k[\boldsymbol{\delta}_k] + \frac{1}{2}D^2\psi_k[\boldsymbol{\delta}_k, \boldsymbol{\delta}_k] + \frac{1}{6}D^3\psi_k[\boldsymbol{\delta}_k, \boldsymbol{\delta}_k, \boldsymbol{\delta}_k] + R_{k+1}$$

where

$$R_{k+1} = \left(\frac{1}{6} \int_0^1 s^3 D^4 \psi(s \mathbf{X}_k^E + (1-s) \mathbf{X}_{k+1}^E) ds \right) [\boldsymbol{\delta}_k, \boldsymbol{\delta}_k, \boldsymbol{\delta}_k, \boldsymbol{\delta}_k]$$

is the remainder term. Therefore, we have

$$\begin{aligned} \psi_{k+1} = & \psi_k + h \mathcal{L}_k \psi_k + h^{\frac{1}{2}} D \psi_k [G_k \boldsymbol{\eta}_{k+1}] + h^{\frac{3}{2}} D^2 \psi_k [\mathbf{F}_k^E, G_k \boldsymbol{\eta}_{k+1}] \\ & + \frac{1}{2} h^2 D^2 \psi_k [\mathbf{F}_k^E, \mathbf{F}_k^E] + \frac{1}{6} D^3 \psi_k [\boldsymbol{\delta}_k, \boldsymbol{\delta}_k, \boldsymbol{\delta}_k] + r_{k+1} + R_{k+1} \end{aligned} \quad (9)$$

where

$$r_{k+1} = \frac{h}{2} (D^2 \psi_k [G_k \boldsymbol{\eta}_{k+1}, G_k \boldsymbol{\eta}_{k+1}] - A : \nabla \nabla \psi_k)$$

Summing Equation (9) over the first K terms, dividing by Kh and use Poisson equation, we have

$$\frac{1}{Kh} (\psi_K - \psi_0) = \frac{1}{K} \sum_{k=0}^{K-1} (\phi_k - \bar{\phi}) + \frac{1}{K} \sum_{k=0}^{K-1} \Delta \mathcal{L}_k \psi_k + \frac{1}{Kh} \sum_{i=1}^3 (M_{i,K} + S_{i,K}), \quad (10)$$

where

$$\begin{aligned} M_{1,K} &= \sum_{k=0}^{K-1} r_{k+1}, \quad M_{2,K} = h^{\frac{1}{2}} \sum_{k=0}^{K-1} D \psi_k [G_k \boldsymbol{\eta}_{k+1}], \quad M_{3,K} = h^{\frac{3}{2}} \sum_{k=0}^{K-1} D^2 \psi_k [\mathbf{F}_k^E, G_k \boldsymbol{\eta}_{k+1}], \\ S_{1,K} &= \frac{h^2}{2} \sum_{k=0}^{K-1} D^2 \psi_k [\mathbf{F}_k^E, \mathbf{F}_k^E], \quad S_{2,K} = \sum_{k=0}^{K-1} R_{k+1}, \quad S_{3,K} = \frac{1}{6} \sum_{k=0}^{K-1} D^3 \psi_k [\boldsymbol{\delta}_k, \boldsymbol{\delta}_k, \boldsymbol{\delta}_k] \end{aligned}$$

Furthermore, it will be convenient to decompose

$$S_{3,K} = M_{0,K} + S_{0,K}$$

where

$$\begin{aligned} S_{0,K} &= h^2 \sum_{k=0}^{K-1} (h D^3 \psi_k [\mathbf{F}_k^E, \mathbf{F}_k^E, \mathbf{F}_k^E] + 3 D^3 \psi_k [\mathbf{F}_k^E, G_k \boldsymbol{\eta}_{k+1}, G_k \boldsymbol{\eta}_{k+1}]) \\ M_{0,K} &= h^{\frac{3}{2}} \sum_{k=0}^{K-1} (D^3 \psi_k [G_k \boldsymbol{\eta}_{k+1}, G_k \boldsymbol{\eta}_{k+1}, G_k \boldsymbol{\eta}_{k+1}] + 3 h D^3 \psi_k [\mathbf{F}_k^E, \mathbf{F}_k^E, G_k \boldsymbol{\eta}_{k+1}]) \end{aligned}$$

Rearrange terms in Equation (9), square on both sides, use Cauchy-Schwarz inequality and take expectation, we have

$$\begin{aligned} \mathbb{E}(\hat{\phi}_K - \bar{\phi})^2 &\leq C_1 \left[\mathbb{E} \frac{(\psi_K - \psi_0)^2}{(Kh)^2} + \frac{1}{K^2} \mathbb{E} \left(\sum_{k=0}^{K-1} (\Delta \mathcal{L}_k \psi_k) \right)^2 + \frac{1}{(Kh)^2} \sum_{i=0}^2 \mathbb{E} S_{i,K}^2 + \frac{1}{(Kh)^2} \sum_{i=0}^3 \mathbb{E} M_{i,K}^2 \right] \\ &= C_1 \left[\mathbb{E} \frac{(\psi_K - \psi_0)^2}{T^2} + \frac{1}{K^2} \mathbb{E} \left(\sum_{k=0}^{K-1} (\Delta \mathcal{L}_k \psi_k) \right)^2 + \frac{1}{T^2} \sum_{i=0}^2 \mathbb{E} S_{i,K}^2 + \frac{1}{T^2} \sum_{i=0}^3 \mathbb{E} M_{i,K}^2 \right] \quad (11) \end{aligned}$$

where $T = kh$, the corresponding time of the underlying continuous dynamics.

We now show how each term is bounded. By Assumption 3, we have

$$\mathbb{E} \frac{(\psi_K - \psi_0)^2}{T^2} \leq \frac{4 \|\psi\|_\infty^2}{T^2} = \mathcal{O}\left(\frac{1}{T^2}\right)$$

The second term $\frac{1}{K^2} \mathbb{E} \left(\sum_{k=0}^{K-1} (\Delta \mathcal{L}_k \psi_k) \right)^2$ is critical in showing the advantage of EWSG, and we will show how to derive its bound in detail later.

The technique we use to bound $\frac{1}{T^2} \mathbb{E} S_{i,K}^2, i = 0, 1, 2$ are all similar, we will first show an upper bound for $|S_{i,K}|$ in terms of powers of $\|\mathbf{F}_k^E\|$, then take square and expectation, and finally expand

squares and use Lemma 5 extensively to derive bounds. As a concrete example, we will show how to bound $\frac{1}{T^2} \mathbb{E} S_{0,K}^2$. Other bounds follow in a similar fashion and details are omitted.

To bound the term containing $S_{0,K}$, we first note that

$$\begin{aligned} |S_{0,K}| &\leq h^2 \sum_{k=0}^{K-1} (h|D^3\psi_k[\mathbf{F}_k^E, \mathbf{F}_k^E, \mathbf{F}_k^E]| + 3|D^3\psi_k[\mathbf{F}_k^E, G_k \boldsymbol{\eta}_{k+1}, G_k \boldsymbol{\eta}_{k+1}]|) \\ &\leq h^2 \|D^3\psi\|_\infty \sum_{k=0}^{K-1} (h\|\mathbf{F}_k^E\|_2^3 + 3\|\mathbf{F}_k^E\|_2\|G_k \boldsymbol{\eta}_{k+1}\|_2^2) \end{aligned}$$

Square both sides of the above inequality and take expectation, we obtain

$$\begin{aligned} &\frac{1}{T^2} \mathbb{E} |S_{0,K}|^2 \\ &\leq \frac{h^4}{T^2} \|D^3\psi\|_\infty^2 \mathbb{E} \left(\sum_{k=0}^{K-1} h\|\mathbf{F}_k^E\|_2^3 + 3\|\mathbf{F}_k^E\|_2\|G_k \boldsymbol{\eta}_{k+1}\|_2^2 \right)^2 \\ &\leq \frac{h^4}{T^2} \|D^3\psi\|_\infty^2 K \sum_{k=0}^{K-1} \mathbb{E} (h\|\mathbf{F}_k^E\|_2^3 + 3\|\mathbf{F}_k^E\|_2\|G_k \boldsymbol{\eta}_{k+1}\|_2^2)^2 \quad (\text{Cauchy-Schwarz inequality}) \\ &= \frac{h^4}{T^2} \|D^3\psi\|_\infty^2 K \sum_{k=0}^{K-1} \mathbb{E} [h^2\|\mathbf{F}_k^E\|_2^6 + 6\|\mathbf{F}_k^E\|_2^4\|G_k \boldsymbol{\eta}_{k+1}\|_2^2 + 9\|\mathbf{F}_k^E\|_2^2\|G_k \boldsymbol{\eta}_{k+1}\|_4^2] \\ &= \frac{h^4}{T^2} \|D^3\psi\|_\infty^2 K \sum_{k=0}^{K-1} h^2 \mathbb{E} \|\mathbf{F}_k^E\|_2^6 + 6\mathbb{E} \|\mathbf{F}_k^E\|_2^4 \mathbb{E} \|G_k \boldsymbol{\eta}_{k+1}\|_2^2 + 9\mathbb{E} \|\mathbf{F}_k^E\|_2^2 \mathbb{E} \|G_k \boldsymbol{\eta}_{k+1}\|_4^2 \\ &= \frac{1}{T^2} \mathcal{O}(K^2 h^4) \\ &= \mathcal{O}(h^2) \end{aligned} \tag{12}$$

To bound the term containing $S_{1,K}$ and $S_{2,K}$, we have

$$\begin{aligned} |S_{1,K}| &\leq \frac{h^2}{2} \sum_{k=0}^{K-1} \|D^2\psi\|_\infty \|\mathbf{F}_k^E\|_2^2 \\ |S_{2,K}| &\leq \frac{1}{24} \|D^4\psi\|_\infty \sum_{k=0}^{K-1} \|\boldsymbol{\delta}_k\|_2^4 \leq \frac{1}{24} h^2 \|D^4\psi\|_\infty \sum_{k=0}^{K-1} \|\sqrt{h}\mathbf{F}_k^E + G_k \boldsymbol{\eta}_{k+1}\|_2^4 \end{aligned}$$

Then we can obtain the following bound in a similar fashion as in Equation (12)

$$\begin{aligned} \frac{1}{T^2} \mathbb{E} S_{1,K}^2 &= \mathcal{O}(h^2) \\ \frac{1}{T^2} \mathbb{E} S_{2,K}^2 &= \mathcal{O}(h^2) \end{aligned}$$

Now we will use martingale argument to bound $\frac{1}{T^2} \mathbb{E} M_{i,K}^2, i = 0, 1, 2, 3$. There are two injected randomness at k -th iteration, the Gaussian noise $\boldsymbol{\eta}_{k+1}$ and the stochastic gradient term determined by the stochastic index I_k . Denote the sigma algebra at k -th iteration by \mathcal{F}_k . For both SGULD and EWSG we have

$$\boldsymbol{\eta}_{k+1} \perp \mathcal{F}_k \text{ and } I_k \perp \boldsymbol{\eta}_{k+1}$$

hence

$$\begin{aligned} \mathbb{E}[\boldsymbol{\eta}_{k+1} | \mathcal{F}_k] &= \mathbf{0} \\ \mathbb{E}[D^3\psi_k[G_k \boldsymbol{\eta}_{k+1}, G_k \boldsymbol{\eta}_{k+1}, G_k \boldsymbol{\eta}_{k+1}] | \mathcal{F}_k] &= 0 \\ \mathbb{E}[D^2\psi_k[\mathbf{F}_k^E, G_k \boldsymbol{\eta}_{k+1}] | \mathcal{F}_k] &= 0 \\ \mathbb{E}[D^3\psi_k[\mathbf{F}_k^E, \mathbf{F}_k^E, G_k \boldsymbol{\eta}_{k+1}] | \mathcal{F}_k] &= 0 \end{aligned}$$

Therefore, it is clear that $M_{i,K}, i = 0, 1, 2, 3$ are all martingales. Due to martingale properties, we have

$$\begin{aligned}\frac{1}{T^2} \mathbb{E} M_{0,K}^2 &= \frac{h^3}{T^2} \sum_{k=0}^{K-1} \mathbb{E} (D^3 \psi_k [G_k \boldsymbol{\eta}_{k+1}, G_k \boldsymbol{\eta}_{k+1}, G_k \boldsymbol{\eta}_{k+1}] + 3h D^3 \psi_k [\mathbf{F}_k^E, \mathbf{F}_k^E, G_k \boldsymbol{\eta}_{k+1}])^2 = \frac{1}{T^2} \mathcal{O}(h^3 K) = \mathcal{O}\left(\frac{h^2}{T}\right) \\ \frac{1}{T^2} \mathbb{E} M_{1,K}^2 &= \frac{1}{T^2} \sum_{k=0}^{K-1} \mathbb{E} r_{k+1}^2 = \frac{1}{T^2} \mathcal{O}(h^2 K) = \mathcal{O}\left(\frac{h}{T}\right) \\ \frac{1}{T^2} \mathbb{E} M_{2,K}^2 &= \frac{h}{T^2} \sum_{k=0}^{K-1} \mathbb{E} (D \psi_k [G_k \boldsymbol{\eta}_{k+1}])^2 = \frac{1}{T^2} \mathcal{O}(h K) = \mathcal{O}\left(\frac{1}{T}\right) \\ \frac{1}{T^2} \mathbb{E} M_{3,K}^2 &= \frac{1}{T^2} h^3 \sum_{k=0}^{K-1} \mathbb{E} (D^2 \psi_k [\mathbf{F}_k^E, G_k \boldsymbol{\eta}_{k+1}])^2 = \frac{1}{T^2} \mathcal{O}(h^3 K) = \mathcal{O}\left(\frac{h^2}{T}\right)\end{aligned}$$

We now collect all bounds derived so far and obtain

$$\begin{aligned}\mathbb{E}(\hat{\phi}_K - \bar{\phi})^2 &\leq C_1 \left[\mathcal{O}\left(\frac{1}{T^2}\right) + \frac{1}{K^2} \mathbb{E} \left(\sum_{k=0}^{K-1} (\Delta \mathcal{L}_k \psi_k) \right)^2 + \mathcal{O}(h^2) + \mathcal{O}\left(\frac{h}{T}\right) + \mathcal{O}\left(\frac{1}{T}\right) + \mathcal{O}\left(\frac{h^2}{T}\right) \right] \\ &\leq C_1 \left[\mathcal{O}\left(\frac{1}{T}\right) + \frac{1}{K^2} \mathbb{E} \left(\sum_{k=0}^{K-1} (\Delta \mathcal{L}_k \psi_k) \right)^2 + \mathcal{O}(h^2) \right] \\ &\leq C_2 \left[\frac{1}{T} + \frac{1}{K^2} \mathbb{E} \left(\sum_{k=0}^{K-1} (\Delta \mathcal{L}_k \psi_k) \right)^2 + h^2 \right]\end{aligned}\tag{13}$$

where $C_2 > 0$ is a constant. In the above inequality, we use $\frac{1}{T^2} < \frac{1}{T}$ and $\frac{h}{T} \leq \frac{1}{T}$, $\frac{h^2}{T} \leq \frac{1}{T}$ as typically we assume $T \gg 1$ and $h \ll 1$ in non-asymptotic analysis.

Now we focus on the remaining term $\frac{1}{K^2} \mathbb{E} \left(\sum_{k=0}^{K-1} \Delta \mathcal{L}_k \psi_k \right)^2$. For SGULD, we have that $\mathbb{E}[\Delta \mathcal{L}_k \psi_k | \mathcal{F}_k] = 0$, hence $\sum_{k=0}^{K-1} \Delta \mathcal{L}_k \psi_k$ is a martingale. By martingale property, we have

$$\frac{1}{K^2} \mathbb{E} \left(\sum_{k=0}^{K-1} \Delta \mathcal{L}_k \psi_k \right)^2 = \frac{1}{K^2} \sum_{k=0}^{K-1} \mathbb{E} (\Delta \mathcal{L}_k \psi_k)^2$$

For EWSG, $\sum_{k=0}^{K-1} \Delta \mathcal{L}_k \psi_k$ is no longer a martingale, but we still have the following

$$\begin{aligned}\frac{1}{K^2} \mathbb{E} \left(\sum_{k=0}^{K-1} \Delta \mathcal{L}_k \psi_k \right)^2 &= \frac{1}{K^2} \sum_{k=0}^{K-1} \mathbb{E} (\Delta \mathcal{L}_k \psi_k)^2 + \frac{2}{K^2} \sum_{i < j} \mathbb{E} (\Delta \mathcal{L}_i \psi_i) (\Delta \mathcal{L}_j \psi_j) \\ &= \frac{1}{K^2} \sum_{k=0}^{K-1} \mathbb{E} (\Delta \mathcal{L}_k \psi_k)^2 + \frac{2}{K^2} \sum_{i < j} \mathbb{E} [(\Delta \mathcal{L}_i \psi_i) \mathbb{E} [\Delta \mathcal{L}_j \psi_j | \mathcal{F}_j]]\end{aligned}\tag{14}$$

For the term $\mathbb{E}[\Delta \mathcal{L}_j \psi_j | \mathcal{F}_j]$, we have

$$\mathbb{E}[\Delta \mathcal{L}_j \psi_j | \mathcal{F}_j] = \mathbb{E}[\langle \nabla V(\boldsymbol{\theta}_j^E) - n \nabla V_{I_j}(\boldsymbol{\theta}_j^E), \nabla_{\mathbf{r}} \psi_j \rangle | \mathcal{F}_j] = \langle \mathbb{E}[\nabla V(\boldsymbol{\theta}_j^E) - n \nabla V_{I_j}(\boldsymbol{\theta}_j^E) | \mathcal{F}_j], \nabla_{\mathbf{r}} \psi_j \rangle$$

as $\psi_j \in \mathcal{F}_j$. Then by Cauchy-Schwarz inequality, Assumption 3 and the fact $\|\nabla V(\boldsymbol{\theta}_j^E) - \mathbb{E}[n \nabla V_{I_j}(\boldsymbol{\theta}_j^E) | \mathcal{F}_j]\|_2 = \mathcal{O}(h)$ as shown in the proof of Theorem 3, we conclude $\mathbb{E}[\Delta \mathcal{L}_j \psi_j | \mathcal{F}_j] = \mathcal{O}(h)$.

Now plug the above result in Equation (14), we have

$$\begin{aligned}
\frac{1}{K^2} \mathbb{E} \left(\sum_{k=0}^{K-1} \Delta \mathcal{L}_k \psi_k \right)^2 &= \frac{1}{K^2} \sum_{k=0}^{K-1} \mathbb{E}(\Delta \mathcal{L}_k \psi_k)^2 + \frac{2}{K^2} \sum_{i < j} \mathbb{E}[(\Delta \mathcal{L}_i \psi_i) \mathbb{E}[\Delta \mathcal{L}_j \psi_j | \mathcal{F}_j]] \\
&= \frac{1}{K^2} \sum_{k=0}^{K-1} \mathbb{E}(\Delta \mathcal{L}_k \psi_k)^2 + \frac{2}{K^2} \sum_{i < j} \mathbb{E}[\Delta \mathcal{L}_i \psi_i] \mathcal{O}(h) \\
&= \frac{1}{K^2} \sum_{k=0}^{K-1} \mathbb{E}(\Delta \mathcal{L}_k \psi_k)^2 + \frac{2}{K^2} \sum_{i < j} \mathcal{O}(h^2) \\
&= \frac{1}{K^2} \sum_{k=0}^{K-1} \mathbb{E}(\Delta \mathcal{L}_k \psi_k)^2 + \frac{2}{K^2} \sum_{i < j} \mathcal{O}(h^2) \\
&= \frac{1}{K^2} \sum_{k=0}^{K-1} \mathbb{E}(\Delta \mathcal{L}_k \psi_k)^2 + \mathcal{O}(h^2)
\end{aligned}$$

Combine both cases of SGULD and EWSG, we obtain

$$\frac{1}{K^2} \mathbb{E} \left(\sum_{k=0}^{K-1} \Delta \mathcal{L}_k \psi_k \right)^2 = \frac{1}{K^2} \sum_{k=0}^{K-1} \mathbb{E}(\Delta \mathcal{L}_k \psi_k)^2 + \mathcal{O}(h^2)$$

Note that $\mathcal{O}(h^2)$ term will later be combined with other error terms with the same order.

The final piece is to bound $\frac{1}{K^2} \sum_{k=0}^{K-1} \mathbb{E}(\Delta \mathcal{L}_k \psi_k)^2$, and we have

$$\begin{aligned}
\frac{1}{K^2} \sum_{k=0}^{K-1} \mathbb{E}(\Delta \mathcal{L}_k \psi_k)^2 &= \frac{1}{K^2} \sum_{k=0}^{K-1} \mathbb{E} \langle \nabla V(\boldsymbol{\theta}_k^E) - n \nabla V_{I_k}(\boldsymbol{\theta}_k^E), \nabla_{\mathbf{r}} \psi_k \rangle^2 \\
&\leq \frac{1}{K^2} \sum_{k=0}^{K-1} \mathbb{E}[\|\nabla V(\boldsymbol{\theta}_k^E) - n \nabla V_{I_k}(\boldsymbol{\theta}_k^E)\|_2^2 \cdot \|\nabla_{\mathbf{r}} \psi_k\|_2^2] \quad (\text{Cauchy-Schwarz inequality}) \\
&\leq \frac{M_3^2}{K^2} \sum_{k=0}^{K-1} \mathbb{E}[\|\nabla V(\boldsymbol{\theta}_k^E) - n \nabla V_{I_k}(\boldsymbol{\theta}_k^E)\|_2^2] \quad (\text{Assumption 3}) \\
&= \frac{M_3^2}{K^2} \sum_{k=0}^{K-1} \mathbb{E}[\mathbb{E}[\|\nabla V(\boldsymbol{\theta}_k^E) - n \nabla V_{I_k}(\boldsymbol{\theta}_k^E)\|_2^2 | \mathcal{F}_k]] \\
&\leq \frac{2M_3^2}{K^2} \sum_{k=0}^{K-1} \mathbb{E}[\underbrace{\mathbb{E}[\|\nabla V(\boldsymbol{\theta}_k^E) - \mathbb{E}[n \nabla V_{I_k}(\boldsymbol{\theta}_k^E) | \mathcal{F}_k]\|_2^2 | \mathcal{F}_k]}_{Q_1} \\
&\quad + \underbrace{\mathbb{E}[\|\mathbb{E}[n \nabla V_{I_k}(\boldsymbol{\theta}_k^E) | \mathcal{F}_k] - n \nabla V_{I_k}(\boldsymbol{\theta}_k^E)\|_2^2 | \mathcal{F}_k]}_{Q_2}]
\end{aligned}$$

The term Q_1 captures the bias of stochastic gradient. For SGULD, uniform gradient subsampling leads to an unbiased gradient estimator, so $Q_1 = 0$ for SGULD. For EWSG, same as in the proof of Theorem 2, we have that

$$\mathbb{E} [\|\nabla V(\boldsymbol{\theta}_k^E) - \mathbb{E}[n \nabla V_{I_k}(\boldsymbol{\theta}_k^E) | \mathcal{F}_k]\|_2^2 | \mathcal{F}_k] = \mathcal{O}(h^2)$$

Combining two cases, we have

$$Q_1 = \mathcal{O}(h^2)$$

For a random vector \mathbf{v} with mean $\mathbb{E}[\mathbf{v}] = \mathbf{0}$, we have

$$\mathbb{E}[\|\mathbf{v}\|^2] = \mathbb{E}[\text{Tr}[\mathbf{v} \mathbf{v}^T]] = \text{Tr}[\mathbb{E}[\mathbf{v} \mathbf{v}^T]] = \text{Tr}[\text{cov}(\mathbf{v})]$$

where $\text{cov}(\mathbf{v})$ is the covariance matrix of random vector \mathbf{v} . Therefore, we have that

$$Q_2 = \text{Tr} [\text{cov}(n \nabla V_{I_k} | \mathcal{F}_k)],$$

i.e., Q_2 is the trace of the covariance matrix of stochastic gradient estimate conditioned on current filtration \mathcal{F}_k .

Combining Q_1 and Q_2 , we have that

$$\begin{aligned} \frac{1}{K^2} \mathbb{E} \left(\sum_{k=0}^{K-1} \Delta \mathcal{L}_k \psi_k \right)^2 &\leq \frac{2M_3^2}{K^2} \sum_{k=0}^{K-1} [\mathbb{E}[\text{Tr}[\text{cov}(n \nabla V_{I_k} | \mathcal{F}_k)]] + \mathcal{O}(h^2)] \\ &= \frac{2M_3^2 h}{T} \frac{\sum_{k=0}^{K-1} \mathbb{E}[\text{Tr}[\text{cov}(n \nabla V_{I_k} | \mathcal{F}_k)]]}{K} + \mathcal{O}\left(\frac{h^3}{T}\right) \end{aligned}$$

Now plug this bound into Equation (13) and we obtain

$$\mathbb{E}(\hat{\phi}_K - \bar{\phi})^2 \leq C \left[\frac{1}{T} + \frac{h}{T} \frac{\sum_{k=0}^{K-1} \mathbb{E}[\text{Tr}[\text{cov}(n \nabla V_{I_k} | \mathcal{F}_k)]]}{K} + h^2 \right]$$

for some constant $C > 0$. ■

E Mini Batch Version of EWSG

When mini batch size $b > 1$, for each mini batch $\{i_1, i_2, \dots, i_b\}$, we use $\frac{n}{b} \sum_{j=1}^b \nabla V_{i_j}$ to approximate full gradient ∇V , and assign the mini batch $\{i_1, i_2, \dots, i_b\}$ probability $p_{i_1 i_2 \dots i_b}$. We can easily extend the transition probability of $b = 1$ to general b , simply by replacing $n \nabla V_i$ with $\frac{n}{b} \sum_{j=1}^b \nabla V_{i_j}$ and end up with

$$\begin{aligned} \tilde{P}(\boldsymbol{\theta}_{k+1}, \mathbf{r}_{k+1} | \boldsymbol{\theta}_k, \mathbf{r}_k) &= \delta(\boldsymbol{\theta}_{k+1} = \boldsymbol{\theta}_k + \mathbf{r}_k h) \times \\ &\quad \sum_{i_1, i_2, \dots, i_b} p_{i_1 i_2 \dots i_b} \Phi(\mathbf{x} + n \mathbf{a}_{i_1 i_2 \dots i_b}) \frac{1}{\sigma \sqrt{h}} \end{aligned}$$

where

$$\mathbf{x} = \frac{\mathbf{r}_{k+1} - \mathbf{r}_k + h \gamma \mathbf{r}_k}{\sigma \sqrt{h}}, \quad \mathbf{a}_{i_1 i_2 \dots i_b} = \frac{\sqrt{h}}{\sigma} \frac{1}{b} \sum_{j=1}^b \nabla V_{i_j}(\boldsymbol{\theta}_k)$$

Therefore, to match the transition probability of underdamped Langevin dynamics with stochastic gradient and full gradient, we let $p_{i_1 i_2 \dots i_b} =$

$$\frac{1}{Z} \exp \left\{ \frac{1}{2} \left[\|\mathbf{x} + n \mathbf{a}_{i_1 i_2 \dots i_b}\|^2 - \|\mathbf{x} + \sum_{i_1 i_2 \dots i_b} \mathbf{a}_{i_1 i_2 \dots i_b}\|^2 \right] \right\}$$

where Z is a normalization constant.

To sample multidimensional random data indices I_1, \dots, I_b from $p_{i_1 i_2 \dots i_b}$, we again use a Metropolis chain, whose acceptance probability only depends on $a_{i_1 i_2 \dots i_b}$ and $a_{j_1 j_2 \dots j_b}$ but not the full gradient.

F EWSG Version for Overdamped Langevin

Overdamped Langevin equation is the following SDE

$$d\boldsymbol{\theta}_t = -\nabla V(\boldsymbol{\theta}_t) dt + \sqrt{2} d\mathbf{B}_t$$

where $V(\boldsymbol{\theta}) = \sum_{i=1}^n V_i(\boldsymbol{\theta})$ and B_t is a d -dimensional Brownian motion. The Euler-Maruyama discretization is

$$\boldsymbol{\theta}_{k+1} = \boldsymbol{\theta}_k - h \nabla V(\boldsymbol{\theta}_k) + \sqrt{2h} \boldsymbol{\xi}_{k+1}$$

where ξ_{k+1} is a d -dimensional random Gaussian vector. When stochastic gradient is used, the above numerical schedme turns to

$$\boldsymbol{\theta}_{k+1} = \boldsymbol{\theta}_k - h \nabla V_{I_k}(\boldsymbol{\theta}_k) + \sqrt{2h} \xi_{k+1}$$

where I_k is the datum index used in k -th iteration to estimate the full gradient.

Denote $\mathbf{x} = \frac{\boldsymbol{\theta}_{k+1} - \boldsymbol{\theta}_k}{\sqrt{2h}}$ and $\mathbf{a}_i = \frac{\sqrt{h} \nabla V_i(\boldsymbol{\theta}_k)}{\sqrt{2}}$. If we set

$$p_i = \mathbb{P}(I_k = i) \propto \exp \left\{ -\frac{\|\mathbf{x} + \sum_{j=1}^n \mathbf{a}_j\|^2}{2} + \frac{\|\mathbf{x} + n\mathbf{a}_i\|^2}{2} \right\}$$

and follow the same steps in the proof of Theorem 2, we will see the transition kernel of full gradient and the transition kernel of stochastic gradient are matched up.

G Variance Reduction

We have seen that when step size h is large, **EWSG** still introduces extra variance. To further mitigate this inaccuracy, we provide in this section a complementary variance reduction technique.

Locally (i.e., conditioned on the state of the system at the current step), we have increased variance

$$\begin{aligned} \text{cov}[\mathbf{r}_{k+1} | \mathbf{r}_k] &= \mathbb{E}[\text{cov}[\mathbf{r}_{k+1} | I]] + \text{cov}[\mathbb{E}[\mathbf{r}_{k+1} | I]] \\ &= h(\Sigma_{k+1}^2 + h \text{cov}[n \nabla V_I(\boldsymbol{\theta}_k)]) \end{aligned} \quad (15)$$

where $\Sigma_{k+1}^2 = \frac{1}{h} \mathbb{E}[\text{cov}[\mathbf{r}_{k+1} | I]]$. The extra randomness due to the randomness of the index I enters the parameter space through the coupling of $\boldsymbol{\theta}$ and \mathbf{r} and eventually deviates the stationary distribution from that of the original dynamics. Adopting the perspective of modified equation [4, 23, 20], we model this as an enlarged diffusion coefficient. To correct for this enlargement and still sample from the correct distribution, we can either, in each step, shrink the size of intrinsic noise to $\Sigma_k \in \mathbb{R}^{d \times d}$ such that $\sigma^2 I = \Sigma_k^2 + h \text{cov}[n \nabla V_I(\boldsymbol{\theta}_{k-1})]$, or alternatively increase the dissipation. More precisely, due to the matrix version fluctuation dissipation theorem $\Sigma^2 = 2\Gamma T$, one could instead increase the friction coefficient $\Gamma \in \mathbb{R}^{d \times d}$ rather than shrinking the intrinsic noise. The second approach is computationally more efficient because it no longer requires square-rooting / Cholesky decomposition of (possibly large-scale) matrices. Therefore, in each step, we set

$$\Gamma_k = \frac{1}{2T}(\sigma^2 I + h \text{cov}[n \nabla V_I(\boldsymbol{\theta}_{k-1})]).$$

Accurately computing $\text{cov}[n \nabla V_I(\boldsymbol{\theta}_{k-1})]$ is expensive as it requires running I through $1, \dots, n$, which defeats the purpose of introducing a stochastic gradient. To downscale the computation cost from $\mathcal{O}(n)$ to $\mathcal{O}(1)$, we use an SVRG type estimation of the this variance instead. More specifically, we periodically compute $\text{cov}[n \nabla V_I(\boldsymbol{\theta}_{k-1})]$ only every L data passes, in an outer loop. In every iteration of an inner loop, which integrates the Langevin, an estimate of $\text{cov}[n \nabla V_I(\boldsymbol{\theta}_{k-1})]$ is updated in an SVRG fashion.

See Algorithm 2 for detailed description. We refer variance reduced variant of EWSG as **EWSG-VR**.

To demonstrate the performance of EWSG-VR, we reuse the setup of simple Gaussian example in subsection 5.1. As shown in Algorithm 2, the only hyper-parameter of EWSG-VR additional to EWSG is the period of variance calibration, for which we set $L = 1$. All other hyper-parameters (e.g. step size h , friction coefficient γ) are set the same as EWSG. We also run underdamped Langevin dynamics with full gradient (FG) using the same hyper-parameters of EWSG. We plot the KL divergence in Figure 5. We see that EWSG-VR further reduces variance and achieves better statistical accuracy measured in KL divergence. Although EWSG-VR periodically use full data set to calibrate variance estimation, it is still significantly faster than the full gradient version. Note that KL divergence of SGLD, pSGLD and SGULD are too large so that we can not even see them in Figure 5

Algorithm 2 EWSG-VR

```

1: Input: {number of data terms  $n$ , gradient functions  $\nabla V_i(\cdot)$ , step size  $h$ , number of data passes  $K$ ,  

   period of variance calibration  $L$ , index chain length  $M$ , friction and noise coefficients  $\gamma$  and  $\sigma$ }
2: initialize  $\boldsymbol{\theta}_0, \mathbf{r}_0, \gamma_0 = \gamma$ 
3: initialize inner loop index  $k = 0$ 
4: for  $l = 1, 2, \dots, K$  do
5:   if  $(l - 1) \bmod L = 0$  then
6:     compute  $\mathbf{m}_1 \leftarrow \mathbb{E}_I[n\nabla V_I(\boldsymbol{\theta}_k)]$ ,  $\mathbf{m}_2 \leftarrow \mathbb{E}_I[n^2\nabla V_I(\boldsymbol{\theta}_k)\nabla V_I(\boldsymbol{\theta}_k)^T]$ 
7:      $\boldsymbol{\omega} \leftarrow \boldsymbol{\theta}_k$ 
8:   else
9:     for  $t = 1, 2, \dots, \lceil \frac{n}{M+1} \rceil$  do
10:     $i \leftarrow$  uniformly sampled from  $1, \dots, n$ , compute and store  $n\nabla V_i(\boldsymbol{\theta}_k)$ 
11:    for  $m = 1, 2, \dots, M$  do
12:       $j \leftarrow$  uniformly sampled from  $1, \dots, n$ , compute and store  $n\nabla V_j(\boldsymbol{\theta}_k)$ 
13:       $i \leftarrow j$  with probability in Equation 6
14:    end for
15:    update  $(\boldsymbol{\theta}_{k+1}, \mathbf{r}_{k+1}) \leftarrow (\boldsymbol{\theta}_k, \mathbf{r}_k)$  according to Equation 4, using  $n\nabla V_i(\boldsymbol{\theta}_k)$  as gradient and
    $\Gamma_k$  as friction
16:     $\mathbf{m}_1 \leftarrow \mathbf{m}_1 + \nabla V_i(\boldsymbol{\theta}_k) - \nabla V_i(\boldsymbol{\omega})$ 
17:     $\mathbf{m}_2 \leftarrow \mathbf{m}_2 + n\nabla V_i(\boldsymbol{\theta}_k)\nabla V_i(\boldsymbol{\theta}_k)^T - n\nabla V_i(\boldsymbol{\omega})\nabla V_i(\boldsymbol{\omega})^T$ 
18:    covar  $\leftarrow \mathbf{m}_2 - \mathbf{m}_1\mathbf{m}_1^T$ 
19:     $\Gamma_{k+1} \leftarrow \frac{1}{2T}(\sigma^2\mathbf{I} + h \text{covar})$ 
20:     $k \leftarrow k + 1$ 
21:  end for
22: end if
23: end for

```

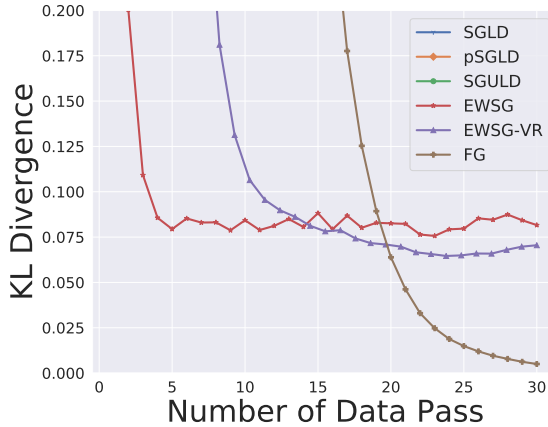


Figure 5: KL divergence

We also consider applying EWSG-VR to Bayesian logistic regression problems. We run experiments on two standard classification data sets `parkinsons`⁶, `pima`⁷ from UCI repository [21].

From Figure 6, we see stochastic gradient methods (SGULD, EWSG and EWSG-VR) only take tens of data passes to converge while full gradient version (FG) requires hundreds of data passes to converge. Compared with SGULD, EWSG produces closer results to FG for which we treat as ground truth, in terms of statistical accuracy. With variance reduction, EWSG-VR is able to achieve even better performance, significantly improving the accuracy of the prediction of mean and standard deviation of log likelihood. It, however, converges slower than EWSG without VR.

One downside of EWSG-VR is that it periodically use whole data set to calibrate variance estimation, so it may not be suitable for very large data sets (e.g. Covertype data set used in subsection 5.3) for

⁶<https://archive.ics.uci.edu/ml/datasets/parkinsons>

⁷<https://archive.ics.uci.edu/ml/datasets/diabetes>

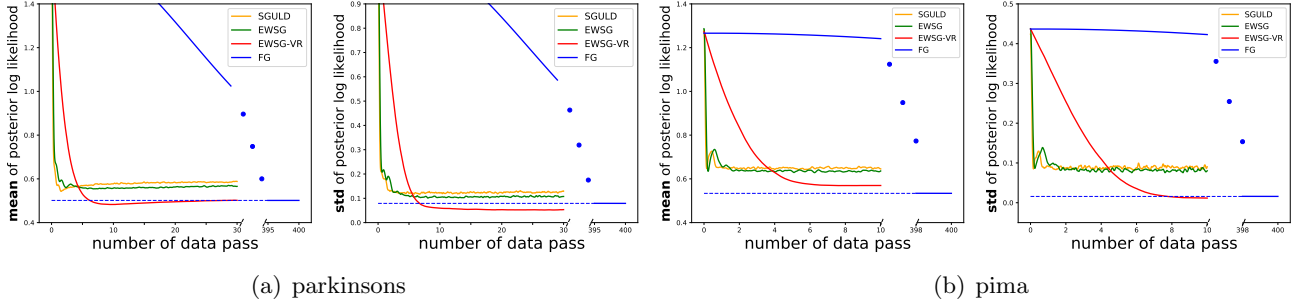


Figure 6: Posterior prediction of mean (*left*) and standard deviation (*right*) of log likelihood on test data set generated by SGULD, EWSG and EWSG-VR on two Bayesian logistic regression tasks. Statistics are computed based on 1000 independent simulations. Minibatch size $b = 1$ for all methods except FG. $M = 1$ for EWSG and EWSG-VR.

which stochastic gradient methods could converge within one data pass.

H EWSG does not necessarily change the speed of convergence significantly

Changing the weights of stochastic gradient from uniform to non-uniform, as we saw, can increase the statistical accuracy of the sampling; however, it does not necessarily increase or decrease the speed of convergence to the (altered) limiting distribution. Numerical examples already demonstrated this fact, but on the theoretical side, we note the non-asymptotic bound provided by Theorem 4 may not provide a tight enough quantification of speed of convergence due to its generality. Therefore, here we quantify the convergence speed on a simple quadratic example:

Consider $V_i(\theta) = \frac{1}{n}(\theta - \mu_i)^2/2$ where μ_i 's are constant scalars. Assume without loss of generality that $\sum_i \mu_i = 0$, and thus $V(\theta) = \sum_{i=1}^n V_i(\theta) = \theta^2/2 + \text{some constant}$. We will show the convergence speed of $\mathbb{E}\theta$ is comparable for uniform and a class of non-uniform SG-MCMC (including EWSG) applied to second-order Langevin equation (overdamped Langevin will be easier and thus omitted):

Theorem 6 Consider, for $0 < \gamma < 2$, respectively SGULD and EWSG,

$$\begin{cases} \theta'_{k+1} = \theta'_k + hr'_k \\ r'_{k+1} = r'_k - h\gamma r'_k - h(\theta'_k - \mu_{I'_k}) + \sqrt{h}\sigma\xi'_{k+1} \end{cases} \quad \text{and} \quad \begin{cases} \theta_{k+1} = \theta_k + hr_k \\ r_{k+1} = r_k - h\gamma r_k - h(\theta_k - \mu_{I_k}) + \sqrt{h}\sigma\xi_{k+1} \end{cases},$$

where I'_k are i.i.d. uniform random variable on $[n]$, I_k are $[\theta, r]$ dependent random variable on $[n]$ satisfying $\mathbb{P}(I_k = i) = 1/n + \mathcal{O}(h^p)$, and ξ_{k+1}, ξ'_{k+1} are standard i.i.d. Gaussian random variables. Denote by $\bar{\theta}'_k = \mathbb{E}\theta'_k$, $\bar{r}'_k = \mathbb{E}r'_k$, $\bar{\theta}_k = \mathbb{E}\theta_k$, $\bar{r}_k = \mathbb{E}r_k$, $x'_k = [\bar{\theta}'_k, \bar{r}'_k]^T$, and $x_k = [\bar{\theta}_k, \bar{r}_k]^T$, then

$$x'_k = (I + Ah)^k x'_0, \quad \text{where } A = \begin{bmatrix} 0 & 1 \\ -1 & -\gamma \end{bmatrix}, \quad (16)$$

for small enough h , $\|x'_k\|$ converges to 0 exponentially with $k \rightarrow \infty$, and x_k converges at a comparable speed in the sense that $\|x_k - x'_k\| = \mathcal{O}(h^p)$ if $x_0 = x'_0$.

Proof: Taking the expectation of the $[\theta', r']$ iteration and using the fact that $\sum_i \mu_i = 0$ and hence $\mathbb{E}\mu_{I'_k} = 0$, one easily obtains (16). The geometric convergence of x'_k thus follows from the fact that eigenvalues of $I + Ah$ have less than 1 modulus for small enough h .

Let $e_k = [0, \mathbb{E}\mu_{I_k}]^T$ and then

$$e_k = [0, \sum_{i=1}^n \mathbb{P}(I_k = i)\mu_i]^T = [0, \mathcal{O}(h^p)]^T$$

Now we take the expectation of both sides of the $[\theta, r]$ iteration and obtain $x_{k+1} = (I + Ah)x_k + he_k$. Therefore

$$x_k = (I + Ah)^k x_0 + (I + Ah)^{k-1} h e_0 + \cdots + (I + Ah) h e_{k-2} + h e_{k-1} = x'_k + h((I + Ah)^{k-1} e_0 + \cdots + (I + Ah) e_{k-2} + e_{k-1})$$

To bound the difference, note $I + Ah$ is diagonalizable with complex eigenvalues $\lambda_{1,2}$ satisfying

$$|\lambda_1| = |\lambda_2| = \sqrt{1 - h\gamma + h^2} = 1 - \gamma h/2 + \mathcal{O}(h^2).$$

Projecting e_j to the corresponding eigenspaces via $e_j = v_{1,j} + v_{2,j}$, we can get

$$\begin{aligned} h\|(I + Ah)^{k-1} e_0 + \cdots + e_{k-1}\| &\leq h \left(\|(I + Ah)^{k-1} e_0\| + \cdots + \|e_{k-1}\| \right) \\ &= h \left(|\lambda_1|^{k-1} \|v_{1,0}\| + |\lambda_2|^{k-1} \|v_{2,0}\| + \cdots + \|v_{1,k-1}\| + \|v_{2,k-1}\| \right) \\ &\leq h C h^p (|\lambda_1|^{k-1} + \cdots + 1) = h C h^p \frac{1 - |\lambda_1|^k}{1 - |\lambda_1|} \leq h C h^p \frac{1}{1 - |\lambda_1|} \\ &\leq \hat{C} h^p \end{aligned}$$

for some constant C and \hat{C} . ■

Important to note is, although this is already a nonlinear example for EWSG (as nonlinearity enters through the μ_{I_k} term), it is a linear example for SGULD. We do not have a tight quantification for the fully nonlinear cases, for which whether EWSG converges faster or comparably like suggested by the experiments remains to be an open theoretical challenge.